Babeș-Bolyai University
Faculty of Chemistry and Chemical Engineering
Supramolecular Organic and Organometallic
Chemistry Centre

Azole-containing organoselenium compounds and their metal complexes. Synthesis, structural characterization and biological activity

PhD Thesis Abstract

Roxana-Alexandra POPA
(married BUTUZA)

Scientific Advisor:
Prof. Dr. Anca Silvestru

Cluj-Napoca
2022

JURY

PRESIDENT

Prof. Dr. Ion Grosu
Faculty of Chemistry and Chemical Engineering, Babeş-Bolyai University, Cluj-Napoca, Romania.

REVIEWERS

Prof. Dr. Vito Lippolis
Dipartimento di Scienze Chimiche e Geologiche, Università degli Studi di Cagliari, Italy.

Prof. Dr. Gabriela-Nicoleta Nemeș
Faculty of Chemistry and Chemical Engineering, Babeş-Bolyai University, Cluj-Napoca, Romania.

Prof. Dr. Cecilia Cristea
Faculty of Pharmacy, Iuliu Haţieganu University of Medicine and Pharmacy, Cluj-Napoca, Romania.

Date of public defence: **9th of December, 2022**

Keywords: organoselenium compounds, group 11 metal complexes, organotin(IV) species, NMR studies, DFT calculations, antioxidant activity, antiproliferative activity

Thesis Table of Contents

Abstract Table of Contents

I. INTRODUCTION

The main objective of the present work is the synthesis, structural characterization and investigation of the potential biological activity of organoselenium compounds containing organic groups with pendant arms capable of intramolecular N···Se or O···Se interactions and/or azole functionalities. By combining selenium, pyrazole or thiazole and, organic groups with pendant arms, we expected to obtain organoselenium compounds with increased stability and valuable biological properties. During the investigation of some peculiar cases, other interesting side studies were developed.

Furthermore, the coordination ability of the obtained diorganoselenium compounds was investigated towards group 11 metals, Cu(II) and Ag(I). The resulting compounds are interesting from both the structural and biological activity point of view, as the silver(I) complexes proved to have promising antiproliferative activity against murine melanoma cells B16.F10.

Finally, a series of tin(IV) bis(organoselenolates) were synthesized starting from the homoleptic diorganodiselenide $(pzCH_2CH_2)_2Se_2$ (pz = pyrazole). The compounds were characterized using appropriate methods and the antiproliferative activity of selected compounds was investigated. NMR spectroscopy proved to be a good tool in the investigation of the coordination geometry of the tin atom in solution, in the study of the solution stability of the compounds and identification of final decomposition products.

III. ORIGINAL CONTRIBUTIONS

III.1. Hetero- and homoleptic diorganoselenides

This subchapter covers the synthesis and structural characterization of some diorganoselenium compounds, as well as the investigation of their potential biological activity, either as antioxidant or antiproliferative agents. A large part of the subchapter is dedicated to the investigation of the diorganoselenoxide intermediates that were observed during the NMR experiments conducted in order to understand the mechanism behind the antioxidant behaviour of these species.

III.1.1. Synthesis and structural characterization

Synthesis

Compounds **1-6** were previously reported by our group when they were synthesized following Method A (**Scheme 10**).[104,105]

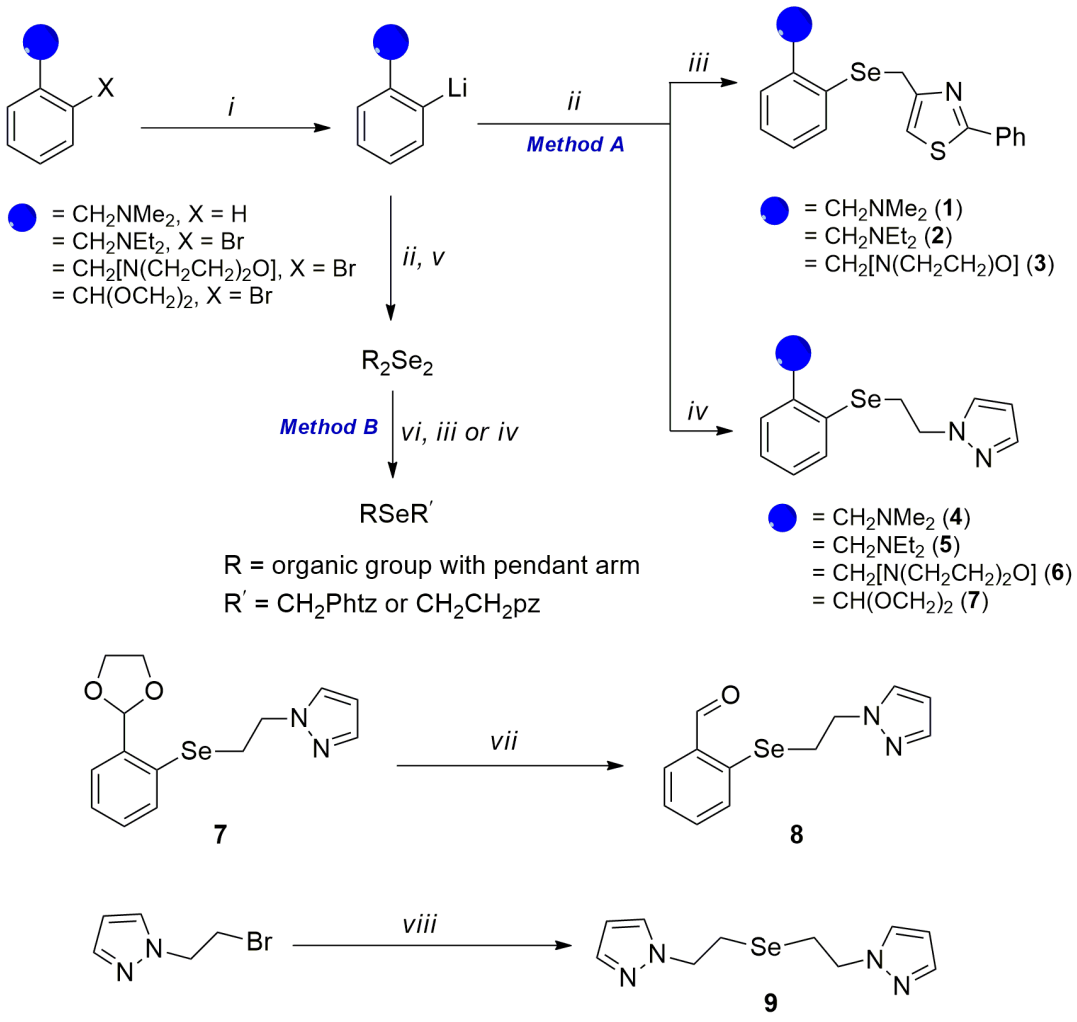

Scheme 10. Synthesis of compounds **1-9**. Reagents and conditions: *i*) ^{n}BuLi, hexane; *ii*) Se, THF; *iii*) PhtzCH$_2$Cl; *iv*) pzCH$_2$CH$_2$Br; *v*) H$_2$O, O$_2$; *vi*) NaBH$_4$, EtOH, 0°C; *vii*) acetone/water, *p*-toluenesulfonic acid; *viii)* Na$_2$Se, water/EtOH, reflux.

The diorganoselenides **2** and **4**-**7** were synthesized for this work *via* Method B, which implies the cleavage of the Se–Se bond in the corresponding bench-stable diorganodiselenides with excess $NaBH_4$ in degassed absolute ethanol at 0°C (ice bath) and reaction of the freshly prepared sodium organoselenolate with the appropriate organic halide, as shown in **Scheme 10**. The novel compound **7** was obtained following both synthetic routes. Compound **8** was obtained by deprotection of the acetal **7** in water/acetone mixture of solvents, under mild acidic conditions. Compound **9** was obtained by reacting freshly prepared Na_2Se with 1-(2-bromoethyl)-1*H*-pyrazole in a water/ethanol mixture, under reflux for 2h.

The target compounds were isolated either as colourless (**1**, **4** and **9**) or yellow solids (**2** and **3**), or as yellow oils (**5**-**8**) in moderate to good yields and are air and moisture-stable. Even though compound **2** was previously reported to be obtained as a yellow oil,[105] it was isolated as a pale-yellow solid. The compounds present a good solubility in most common organic solvents.

NMR spectroscopy

All the compounds were characterized in solution by multinuclear NMR spectroscopy (^1H, $^{13}C\{^1H\}$, $^{77}Se\{^1H\}$). The resonance signals present in the ^1H and $^{13}C\{^1H\}$ NMR spectra were assigned using two-dimensional NMR experiments (COSY, HSQC, HMBC). For the previously reported compounds **1**-**6** the NMR spectra in $CDCl_3$ are in agreement with the published data.[104,105] However, the room temperature ^1H NMR spectra of the compounds does not bring evidence for the presence of N···Se interaction in solution, as only one set of resonance signals was observed for the $–CH_2NR_2$ moiety (NR_2 = NMe_2, NEt_2, $N(CH_2CH_2)_2O$).

In the ^1H NMR spectrum of compound **7**, a multiplet signal corresponding to the ethylene protons in the dioxolan group is observed at 4.01-4.18 ppm. The singlet resonance signal corresponding to H_7 (6.1 ppm) in compound **7** is shifted to 10.2 ppm in the ^1H NMR spectrum of compound **8**, a characteristic chemical shift for C*H*O proton, while the multiplet resonance signal disappears, thus confirming the complete deprotection of the formyl group (**Figure 8**). In the $^{77}Se\{^1H\}$ NMR spectra of compounds **7** and **8**, singlet resonances are present at 229.1 ppm and 301.6 ppm, respectively, in the specific range for aryl alkyl diorganoselenide species.

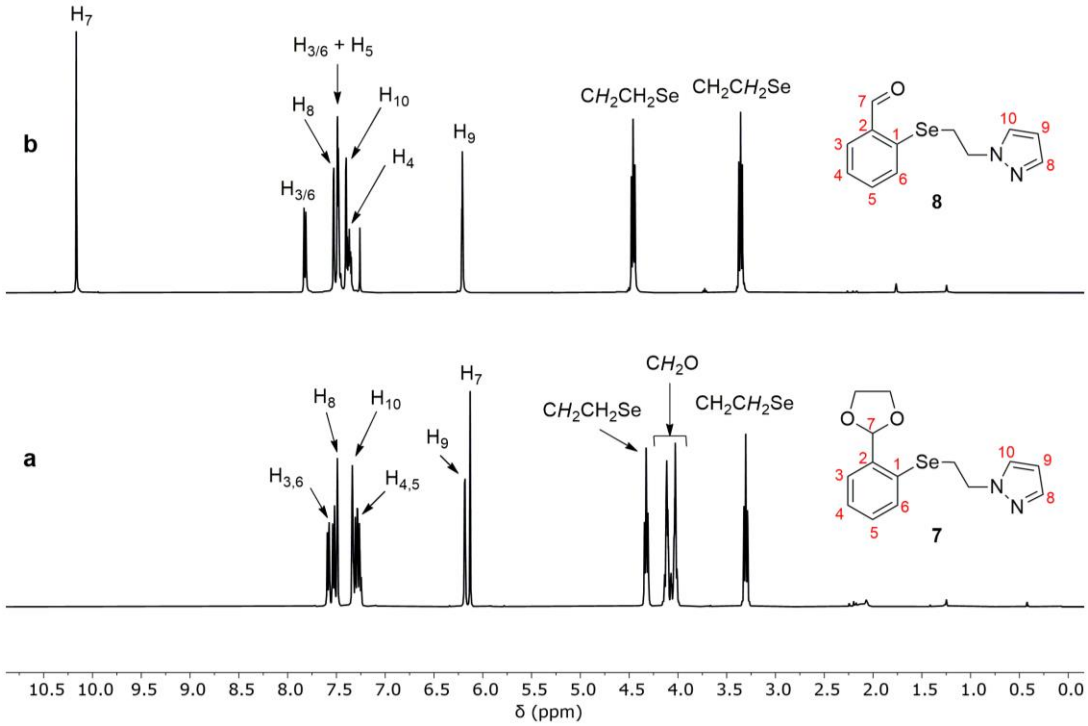

Figure 8. Stacked ^{1}H NMR spectra ($CDCl_3$) of (a) compound **7** and (b) compound **8**.

The ^{1}H NMR spectrum of compound **9** shows two triplet resonance signals in the aliphatic region that were assigned to the –C*H*$_2$C*H*$_2$– protons, a triplet resonance signal at 6.22 ppm, which is characteristic for the pz-*H*$_2$ proton, and two doublet resonance signals that were assigned to the other two protons in the pyrazole ring (**Figure 9**). The ^{77}Se{^{1}H} NMR spectrum presents one resonance signal at 128.3 ppm, which is in the characteristic region for a diorganoselenide with alkyl substituents.

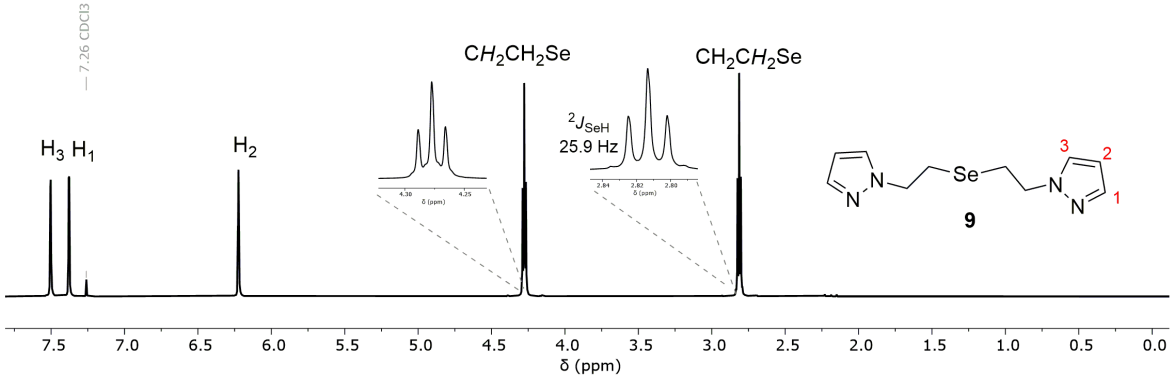

Figure 9. ^{1}H NMR spectrum ($CDCl_3$) of compound **9**.

Mass spectrometry

In the ESI+ mass spectrum of compound **7** the pseudo-molecular ion corresponds to $[M + Na]^+$ at *m/z* 347.02717, while in APCI+ MS spectrum of compound **8**, the base peak corresponds to $[M – CH_2CH_2pz]^+$ at *m/z* 184.9508. For compound **9** the ESI+ mass spectrum

shows the pseudo-molecular peak that corresponds to $[M + H]^+$ at *m/z* 271.04773 and another peak corresponding to $[M – CH_2CH_2pz]^+$ at *m/z* 174.97647.

X-ray diffraction studies

The molecular structures of compounds **1** and **4** were previously reported by our group,[104] and showed the presence of intramolecular N···Se interaction between the nitrogen atom in the pendant arm and the chalcogen atom. For compound **3** suitable crystals for single-crystal X-ray diffraction were obtained during this work by slow diffusion of dichloromethane into a hexane solution of the compound. In this case as well, the molecular structure reveals an intramolecular coordination of the nitrogen atom in the morpholinyl ring to the selenium atom (N1···Se1 2.962 Å *vs*. Σr_{vdW}(Se,N) = 3.54 Å[58]), thus giving rise to a distorted T-shaped coordination geometry about the selenium atom (N1–Se1–C12 171.70°), as shown in **Figure 11**. As a result, the compound can be described as a neutral, hypercoordinated *10–Se–3* species. The N···Se interaction in **3** has a similar value as that found in other diorganoselenium(II) species with *C,N* chelating organic groups, *e.g.* 2.836(3) Å in $[2\text{-}(Me_2NCH_2)C_6H_4]SeCH_2Phtz$ (**1**) and 3.093(3) Å in $[2\text{-}(Me_2NCH_2)C_6H_4]SeCH_2CH_2pz$ (**4**),[104] 2.982(8) Å in $[2\text{-}(Me_2NCH_2)C_6H_4]SeCH_2CH_2(3,5\text{-}dmpz)$,[52] 3.190/3.099 Å in $[2\text{-}(Me_2NCH_2)C_6H_4]_2Se$,[48] 3.179/3.097 Å in $[2,6\text{-}(Me_2NCH_2)_2C_6H_4]_2Se$.[106]

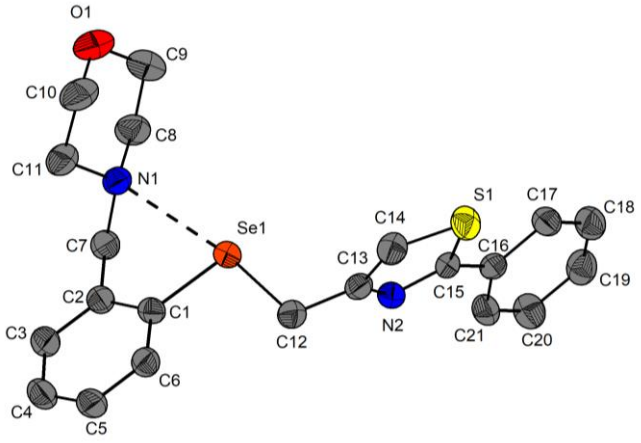

Figure 11. Thermal ellipsoids representation of compound **3** with ellipsoids at the 30% probability level. Hydrogen atoms were omitted for clarity.

The intramolecular interaction generates a non-planar five-membered SeC_3N ring which is folded about the imaginary C7···Se axis, thus inducing planar chirality. As a result, the compound crystallizes as a mixture of R_{N1} and S_{N1} isomers. Separate zig-zag polymeric chains of R_{N1}-**3** and S_{N1}-**3** isomers are generated through π H···Cg′ (C16′–C21′)

intermolecular interactions with a value of 2.92 Å (<3.0 Å, γ = 16.4° < 30°[107,108]) between a methylene proton in the morpholinyl group and the phenyl ring in the phenylthiazole group of a neighbouring molecule. The morpholinyl ring has a chair conformation, with O1 and N1 in apices.

III.1.2. Evaluation of GPx-like activity

The potential antioxidant activity of the pyrazole derivatives **4**-**7** and **9** was explored by measuring the time required to reduce the concentration of the thiol by 50% (T_{50}) determined according to the Tomoda method[47,74] using tiophenol as a glutathione alternative. The reaction was followed by UV-Vis spectroscopy at 305 nm, maximum absorption wavelength of PhSSPh.

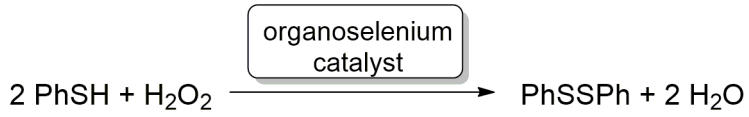

Table 4 centralizes the calculated T_{50} values and the efficiency relative to Ebselen. Overall, the tested diorganoselenides showed only a moderate antioxidant activity when compared to the related diorganodiselenides and Ebselen. For the tested series the antioxidant decreases in the order **5** > **4** ≈ **9** > **6** ≈ **7**, but only compound **5** had a slightly better antioxidant activity than Ebselen.

Table 4. T_{50} values of tested organoselenium compounds.

Catalyst[a]	T_{50} (min)[b,c]	Efficiency relative to Ebselen
4	174.52 (±16.46)	0.88
5	127.54 (±0.93)	1.20
6	197.40 (±21.37)	0.78
7	199.31 (±11.43)	0.77
9	176.18 (±5.85)	0.87
$[2\text{-}(Me_2NCH_2)C_6H_4]_2Se_2$	2.29 (±0.05)	67.4
$[2\text{-}\{(CH_2O)_2CH\}C_6H_4]_2Se_2$	15.91 (±0.87)	9.69
Ebselen[110]	154.26 (±6.35)[110]	1.00
Ph_2Se_2[110]	55.04 (±3.50)[110]	2.80

[a] *Assay conditions: MeOH, catalyst (0.1 mM), PhSH (2 mM), H_2O_2 (5 mM)*
[b] *T_{50} the time necessary to reduce the thiol concentration by 50% upon addition of H_2O_2*
[c] *Standard deviations are given in brackets.*

Investigation of reaction mechanism

The reactions between the organoselenium compounds and H_2O_2, as well as that between the resulting intermediate and PhSH, in methanol-d_4 were followed by $^{77}Se\{^1H\}$

and ^{1}H NMR spectroscopy. The obtained results are in accordance with other literature data[111,112] and show that the reactions are reversible and they occur *via* a selenoxide intermediate (**Scheme 11**).

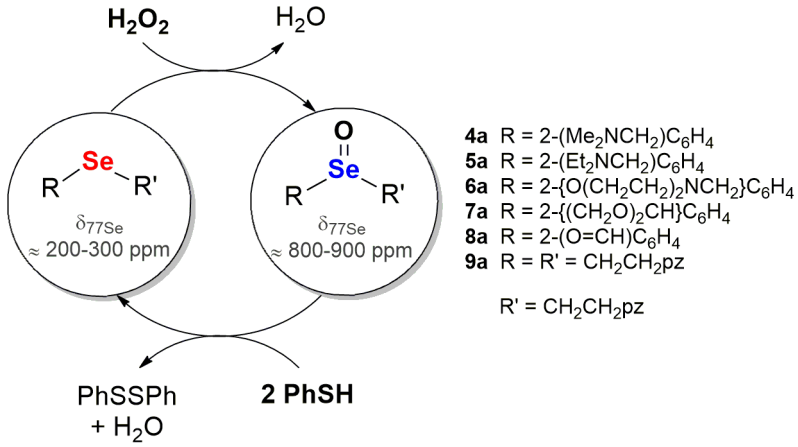

Scheme 11. Inter-conversion between diorganoselenides and diorganoselenoxides.

Upon addition of H_2O_2 to the organoselenium compound the chemical shift in the ^{77}Se{^{1}H} NMR spectra shifts downfield to a value corresponding to a diorganoselenoxide species (**Table 5**) and when PhSH (2 equiv.) is added the signal shifts back to the initial value, thus confirming the re-formation of the diorganoselenides. In all cases, the diorganoselenoxide intermediate appears to be stabilized by intramolecular interactions.

Table 5. ^{77}Se{^{1}H} NMR chemical shifts of compounds **4**-**9** and **4a**-**9a** in methanol-d_4.

Diorganoselenide	^{77}Se{^{1}H} NMR δ (ppm)	Diorganoselenoxide	^{77}Se{^{1}H} NMR δ (ppm)
4	233.8	**4a**	821.4
5	237.1	**5a**	819.4
6	241.6	**6a**	824.1
7	224.8	**7a**	835.1
8	302.3	**8a**	804.7
9	138.5	**9a**	852.6

Upon addition of H_2O_2 (2 equiv.) to a methanol-d_4 solution of diorganoselenide **4**, two species can be observed in approximately 1:1 ratio after 30 min, and after another 20 min only one species is present, namely the diorganoselenoxide **4a**. When PhSH (2 equiv.) was added to the resulting solution, the re-formation of diorganoselenide **4** could be observed together with the formation of PhSSPh and two additional minor species (**Figure 14**).

In the aliphatic region of the ^{1}H NMR spectrum of diorganoselenoxide **4a** the presence of an AB spin system for the CH_2 protons in the pendant arm and four multiplet

signals corresponding to the four non-equivalent protons in the ethylene group (**Figure 15**) suggest the presence of two N···Se intramolecular interactions in the molecule.

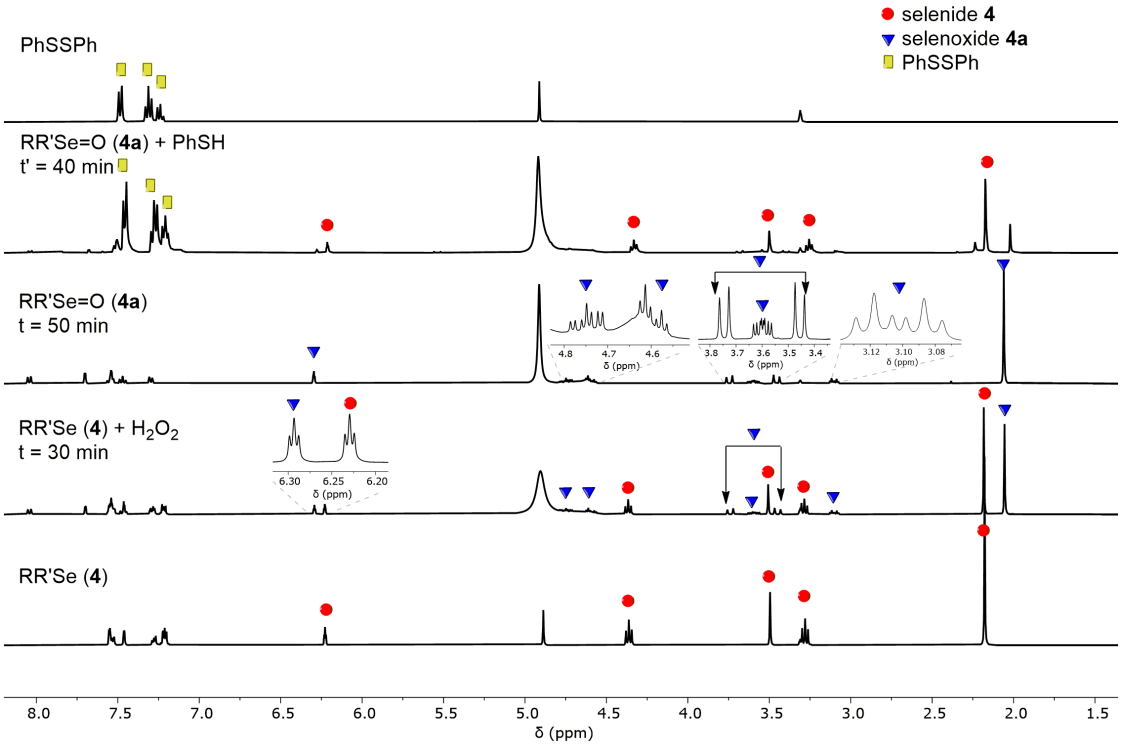

Figure 14. Reaction mechanism of compound **4** followed by ^{1}H NMR (methanol-d_4) spectroscopy and ^{1}H NMR spectrum of PhSSPh (methanol-d_4).

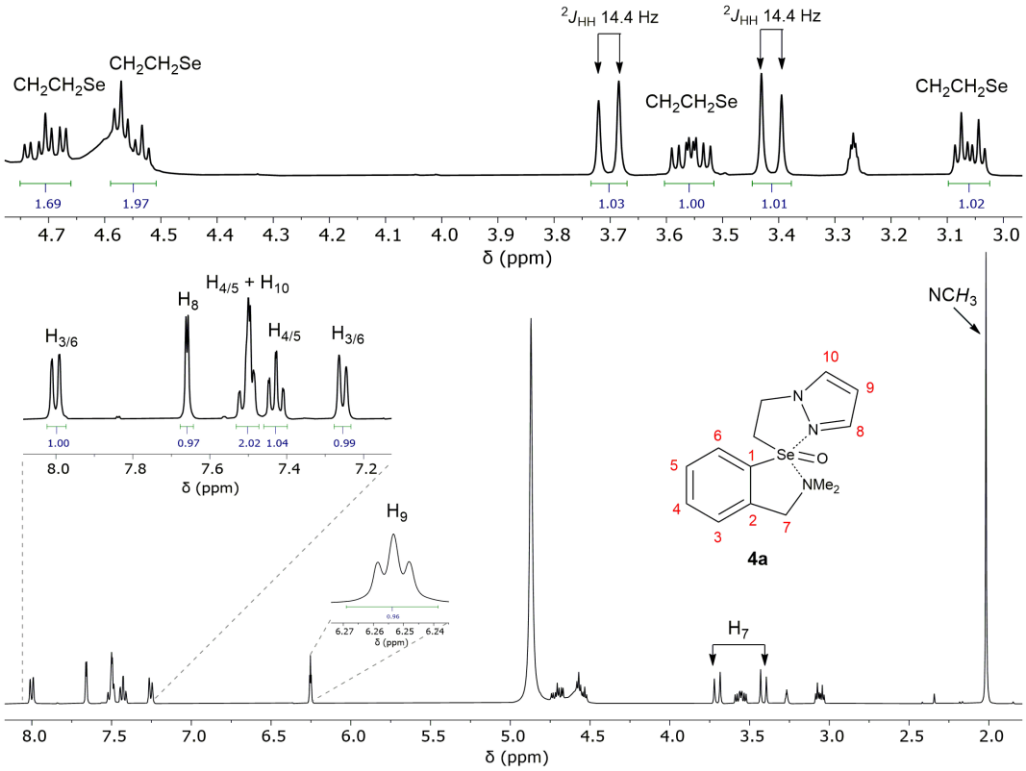

Figure 15. ^{1}H NMR (methanol-d_4) spectrum of **4a** and details of the aliphatic and aromatic regions.

The ^{1}H NMR spectra of diorganoselenoxides **5a** and **6a** present the same type of multiplet resonance signals for the four hydrogen atoms in the –C*H*$_2$C*H*$_2$– moiety and an AB spin system for the methylene protons in the pendant arm. In addition, two sets of characteristic multiplet signals for the hydrogen atoms in the ethyl and morpholinyl moieties, respectively, are present. It is worth mentioning that these species are less stable than diorganoselenoxide **4a** in solution, therefore complete NMR data could not be obtained for them. The ^{1}H NMR spectra suggested that diorganoselenoxides **7a** and **8a** resulted in a mixture with other compounds, but only one diorganoselenoxide species as seen in the ^{77}Se{^{1}H} NMR spectra.

After addition of H_2O_2 (2 equiv.) to compound (pzCH$_2$CH$_2$)$_2$Se (**9**), the complete formation of (pzCH$_2$CH$_2$)$_2$Se(O) (**9a**) was observed after 15 min (^{1}H and ^{77}Se{^{1}H} NMR spectra). Within a few minutes of addition of PhSH (2 equiv.) the diorganoselenoxide has completely reacted and the diorganoselenide was reformed, together with PhSSPh (**Figure 18**). The three broad resonances in the aliphatic region of the ^{1}H NMR spectrum of **9a**, which were assigned to the –C*H*$_2$C*H*$_2$– protons, indicate a fluxional behaviour of the compound in solution with only one pyrazole ring alternatively coordinated to the selenium center.

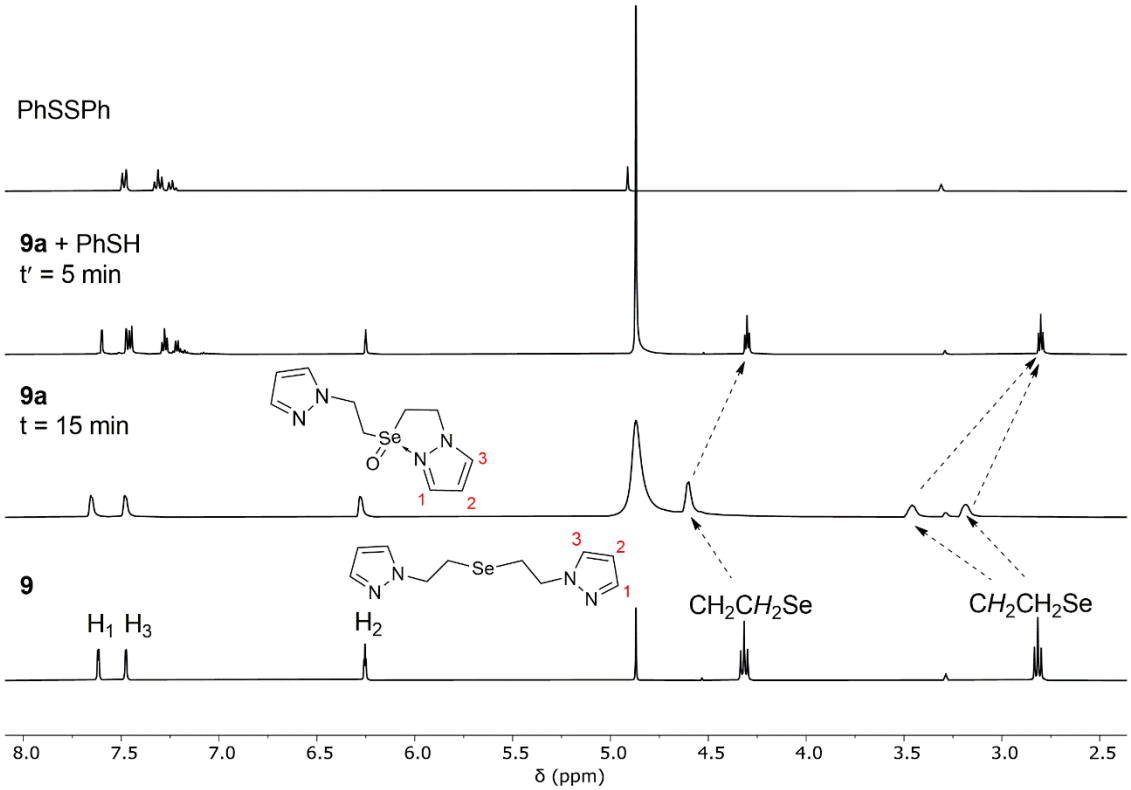

Figure 18. Reaction mechanism of compound **9** followed by ^{1}H NMR (methanol-d_4) spectroscopy and ^{1}H NMR spectrum (methanol-d_4) of PhSSPh.

The kinetic profile for the oxidation of **4** to **4a** (**Figure 20**) shows an inverse sigmoidal relation between the diorganoselenide and the diorganoselenoxide. After a relatively short lag-phase that lasted about 20 min, the NMR resonance signals of **4** started to decrease more rapidly with the simultaneous appearance of new multiplets that were assigned to diorganoselenoxide **4a**. This behavior might suggest that the oxidized product acts as a catalyst for the first step of the reaction.

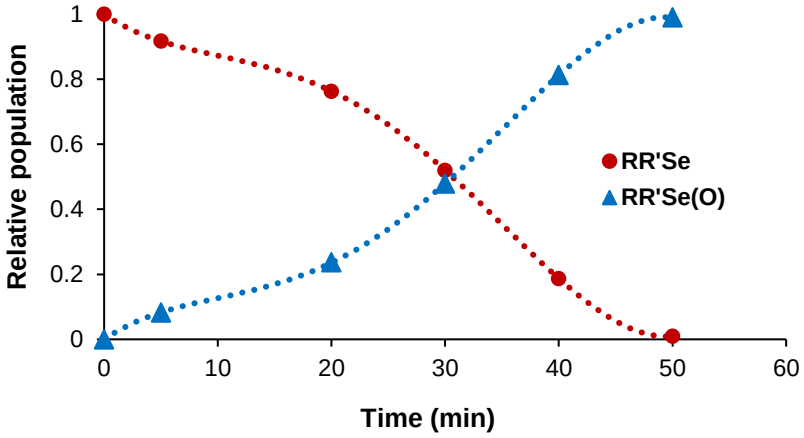

Figure 20. Representation of the kinetic profile derived from the normalized areas of selected ^{1}H NMR resonance signals (δ = 6.23 ppm for diorganoselenide **4** and δ = 6.29 ppm for diorganoselenoxide **4a**, corresponding to pz-H_9).

Cyclic voltammetry

The electrochemical properties of selected compounds **4-6** and **9** were investigated in methanol with gold and glassy carbon working electrodes. The applied potential range was chosen in such a way as to evidence oxidation to Se(IV) species (diorganoselenoxides) and Se(VI) species (diorganoselendioxides), and in order to avoid solvent oxidation and reduction to Se(0).

Figure 21 presents the cyclic voltammograms of the compounds on the gold electrode. Generally, the obtained voltametric peaks are irreversible and only compound **5** shows a small cathodic peak associated to the second oxidation. For compounds **4** and **5,** a clear two step oxidation can be observed, indicating the stability of the corresponding diorganoselenoxide species **4a** and **5a** in the potential range between the successive oxidation peaks, while for diorganoselenides **6** and **9**, a single oxidation peak can be observed, which indicates that the diorganoselenoxides are further oxidized to diorganoselendioxides.

The potentials for the peak associated with the first oxidation step to Se(IV) species (diorganoselenoxides) are in the range of +0.95 to +1.0 V *vs.* Ag/AgCl, while the total

oxidation to diorganoselendioxide takes place in the range of +1.1 to +1.5 V *vs.* Ag/AgCl. Compounds **4** and **5** were the most promising, in agreement with the results obtained for T_{50}.

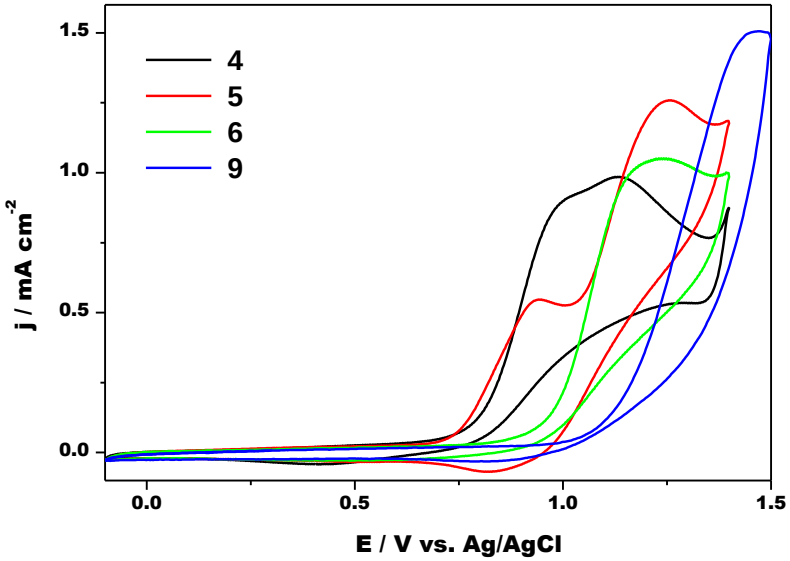

Figure 21. Cyclic voltammograms of the diorganoselenides **4**-**6** and **9**. Gold electrode, 100 mV·s^{-1} scan rate. Concentrations: **4**, 2.6 mM; **5**, 2.45 mM; **6**, 2.34 mM; **9**, 3.03 mM.

DFT calculations

In order to better understand the nature and implication of the N···Se interactions on the stability of the diorganoselenoxide species **4a**-**9a**, DFT calculations were performed using the PBE1PBE 6-31G(d,p)/Grimme's dispersion (D3 version) setup. **Scheme 12** shows the proposed structures of the diorganoselenoxides based on the conclusions drawn from the experimental NMR spectra.

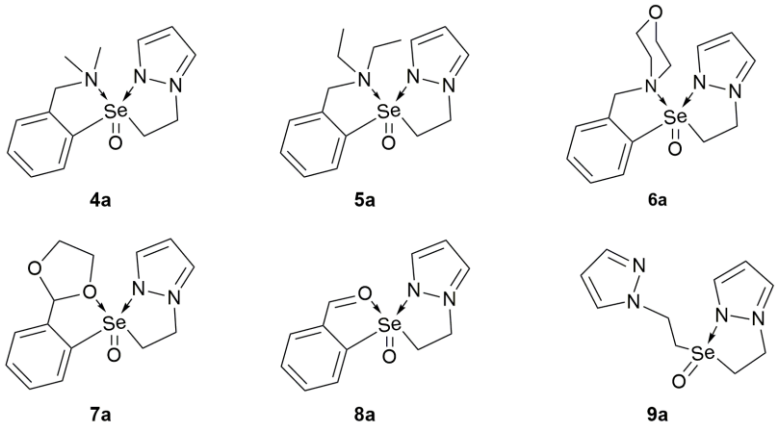

Scheme 12. Proposed structures for diorganoselenoxides **4a**–**9a** with two intramolecular N···Se interactions for species **4a**-**8a** and one interaction for **9a**.

DFT calculations were carried out both in gas phase and in methanol solution (SCRF IEF-PCM) and a series of parameters were evaluated in relation to the strength of the interaction – interatomic distance, Wiberg bond indexes (WBIs),[118] and interaction energies.

The results for the geometry optimization in gas phase and in methanol solvent are centralized in **Table 8**. The optimized geometry of diorganoselenoxide **4a** in methanol showing the two N···Se interactions is depicted in **Figure 22.**

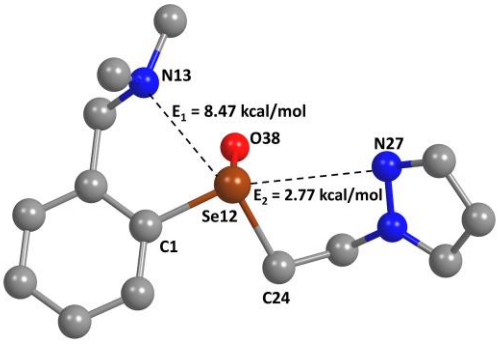

Figure 22. DFT-optimized structure of diorganoselenoxide **4a**, in methanol. Hydrogen atoms were omitted for clarity. Bond distances (Wiberg bond indexes in parentheses): N13–Se12 2.760 Å (0.057), N27–Se12 3.173 Å (0.019).

Detailed studies on systems with intramolecular nonbonding heteroatom-chalcogen interactions suggest that the interaction between the heteroatom's (N or O) lone pair orbital and an antibonding σ^*_{Se-X} orbital leads to a weak unsymmetrical hypervalent bond.[55,120,121]

Generally, the orbital interaction between the donor lone pair and the Se–X (X = C, halogen, etc.) antibonding orbital is maximized by the collinear geometry between the donor atom (Y) and the σ^*_{Se-X} acceptor orbital. Depending on the strength of the Y···Se interaction, the Y···Se–X angle ranges from 165° to 180°, the stronger the interaction, the more linear the angle. In the present study, Y···Se–X angles range from 163° to 171° for the interaction between the heteroatom (N or O) in the pendant arm and the selenium atom, while for the interaction involving the nitrogen atom from the pyrazole ring the angles are even more deviated from linearity (158°–161°). The big deviation from linearity in some cases suggest weak interactions or the absence of them.

The value of the interaction energy involving the donor atom in the pendant arm (6.6-10.1 kcal·mol^{-1} in methanol) indicates a weak or medium-weak interaction for diorganoselenoxides **4a**-**6a** and **8a**, but extremely weak, if not absent, for **7a** and **9a**. A very weak interaction was evidenced between the nitrogen atom of the pyrazole ring and selenium, the interaction energies being in the range 1.6-2.8 kcal·mol^{-1} in methanol. When comparing the optimized interatomic distances and interaction energies in the gas phase and in solution, it is visible that solvation favours the stronger interaction, while decreasing the weaker interaction.

The molecular orbitals (MO) containing the lone pairs of electrons from the nitrogen atoms, both in the pendant arm and in the pyrazole ring, are properly oriented towards the unoccupied antibonding molecular orbitals on the selenium atom, thus making possible the existence of the intramolecular interaction. The molecular orbitals capable of accepting electrons are antibonding σ^*_{Se-C} orbitals.

For compound **9a**, the optimized geometry shows only one weak N···Se intramolecular nonbonding interaction (1.59 kcal/mol) with one pyrazole ring in the interaction favourable position while the other pyrazole ring is flipped with the nitrogen atom in the opposite direction.

Understanding the nonbonding interaction in the studied systems

Calculations for diorganoselenoxides **4a** and **9a** were extended to the species displaying only the strongest interaction for **4a**, two interactions for **9a** or no interaction at all, and the natural bond orbital (NBO) analysis was carried out.

In comparison with the unperturbed situation, a slight lengthening of the Se=O bond was observed in the optimized structures. From an energy point of view the presence of two, one or no N→Se interactions does not affect significantly the stability of the diorganoselenoxide, the optimized structure of **4a** featuring two intramolecular interactions being only 1.88 kcal·mol^{-1} more stable than the structure featuring no interactions, while for compound **9a** the species with only one N→Se interaction was found to be the most stable one, as it was assumed from the experimental NMR data.

In conclusion, NBO analysis suggests that the N→Se interaction present in these compounds has a mainly covalent character, rather than electrostatic, and originates from a charge transfer (CT) interaction between a lone pair of electrons on the donor atom and an antibonding orbital on selenium (σ^*_{Se-C}).

III.1.3. Evaluation of antiproliferative activity

The phenylthiazole derivatives **1-3** were screened for antiproliferative activity against murine melanoma B16.F10 cells using the ELISA-BrdU colorimetric assay. The effects of various concentrations of the compounds on cancer cell proliferation are presented in **Figure 27**. The cytotoxic effect of the compounds on B16.F10 cells were similar and correlated positively with the concentrations tested (r = 0.98 for **1**; r = 0.98 for **2**). Our finding was also supported by calculation of IC_{50} values for these compounds (**Table 10**). The methyl and ethyl analogues show similar good activity in comparison with the standard drug Dacarbazine.[124] However, upon replacing the NR_2 (R = Me, Et) group in the pendant arm

with a bulkier substituent (morpholinyl) the activity is practically lost, as compound **3** did not show antiproliferative activity for concentrations up to 300 μM.

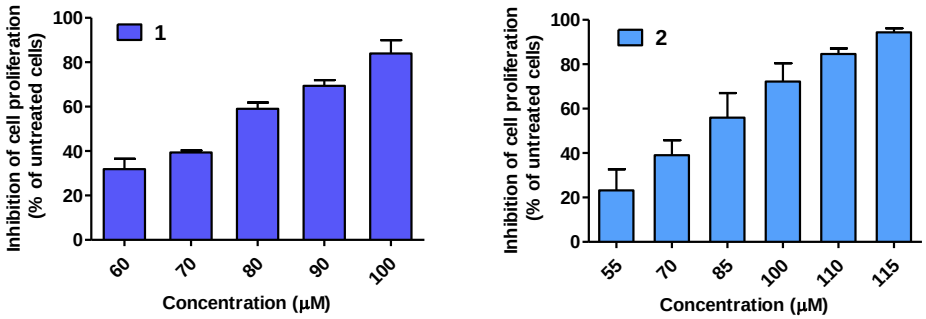

Figure 27. Concentration-dependent antiproliferative effect of compounds **1** and **2** in comparison with untreated B16.F10 control cells.

Table 10. Antiproliferative effect of compounds **1**-**2** on murine melanoma B16.F10 cells.

Compound	**1**	**2**	Dacarbazine
IC_{50} (μM)	84.36	82.9	149.7 ± 1.9

Pyrazole derivatives **4**-**9** were screened for antiproliferative activity against the mouse colon carcinoma C26 cell line using the ELISA-BrdU colorimetric assay. Unfortunately, for concentrations up to 300 μM of compounds **4** and **5**, treated cells proliferated comparatively to the untreated colon carcinoma C26 cells. For a value above this concentration, it was considered that the compounds have no antiproliferative activity against this type of cells.

The IC_{50} value could be calculated only for the morpholinyl derivative **6** (IC_{50} = 200.4 μM), but the value is much higher than that of the standard drugs 5-fluorouracil (IC_{50} = 5.38 μM) and that of Deltonin (IC_{50} = 1.22 μM),[125] rendering this compound practically inactive as well.

III.2. Group 11 metal complexes with diorganoselenides as neutral ligands

This subchapter comprises the results obtained from the investigation of the coordination ability of the diorganoselenium ligands **1-9** towards *d* metals. The ligands were reacted with various Ag(I), Cu(I) and Cu(II) salts in 1:1 ligand to metal salt molar ratio. A series of novel metal complexes were obtained and characterized through multinuclear NMR spectroscopy (^{1}H, ^{13}C{^{1}H}, ^{19}F{^{1}H}, ^{77}Se{^{1}H}), mass spectrometry, elemental analysis, IR and UV-Vis spectroscopy, molar conductivity measurements and single-crystal X-ray diffraction, as appropriate for each complex.

III.2.1. Silver(I) complexes of heteroleptic ligands

Synthesis

The heteroleptic diorganoselenides **1-6** were reacted with AgOTf in 1:1 molar ratio in acetone at room temperature (**Scheme 13**). Precautions were taken in order to avoid exposure to light, but no special measures were taken in order to avoid air or moisture.

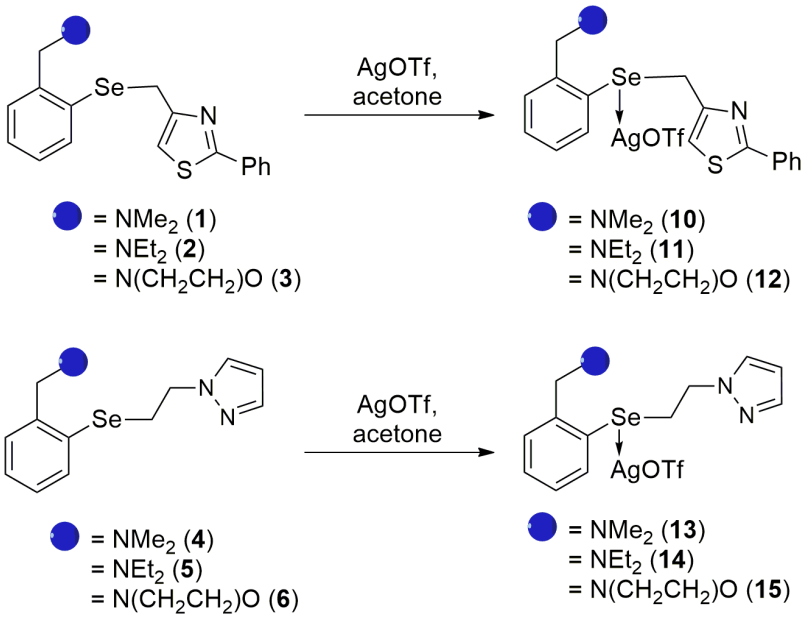

Scheme 13. Synthesis of silver(I) complexes **10-15**.

After evaporation of the solvent and washing with diethyl-ether, the silver(I) complexes **10-15** were isolated as air-stable light-sensitive colourless and pale-yellow solids in good to excellent yields. Over time, the phenylthiazole derivatives are more stable than the pyrazole derivatives, which start to slowly decompose after a few months in air in the absence of light.

When attempting to obtain complex **16** by reacting ligand **7** with AgOTf in acetone or methanol, a mixture of compounds **16** and **17** was obtained (**Scheme 14**). Further attempts

to isolate complex **16** from the mixture were not made. Complex **17** was obtained as a colourless solid by reacting ligand **8** with AgOTf in acetone in the absence of light.

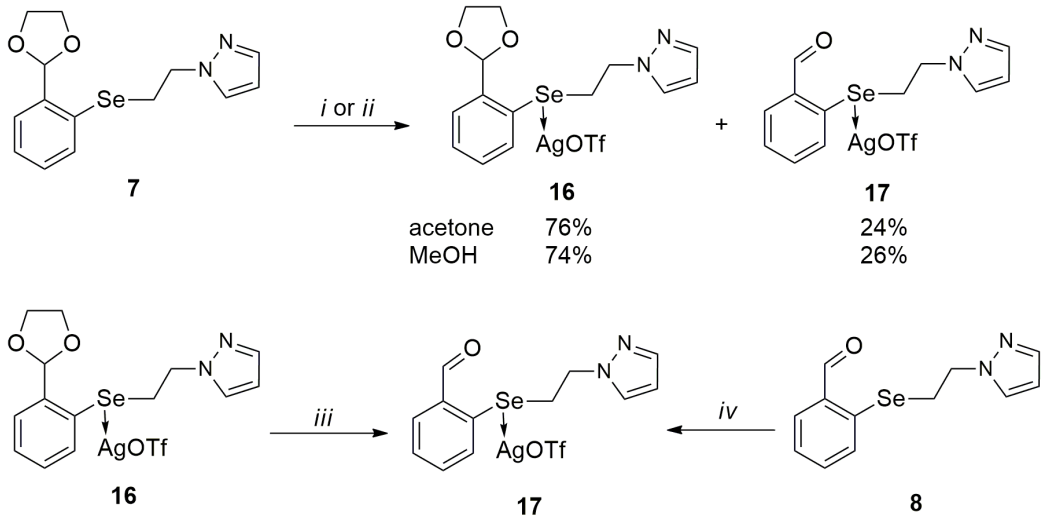

Scheme 14. Reaction scheme for complexes **16** and **17**. Reagents and conditions: *i*) AgOTf, acetone, 40 min; *ii*) AgOTf, MeOH, 20 min; *iii*) acetone, 2 days; *iv*) AgOTf, acetone, 40 min.

NMR spectroscopy

Compounds **10** and **12** were completely soluble in acetone-d_6, while compound **11** was only slightly soluble. Hence, the final spectra of this compound were recorded in DMSO-d_6. **Figure 29** shows the stacked ^{1}H NMR spectra of ligand **2** and complex **11**. In comparison to the corresponding ligands, the resonance signals are downfield shifted. The singlet resonance signal corresponding to the methylene protons in the pendant arm appears slightly broadened, indicating a possible rapid coordination-decoordination process.[55] In all three cases, the ^{1}H NMR spectra brings no clear evidence for the presence of N···Se or N···Ag interactions in solution. The ^{77}Se{^{1}H} NMR spectra show one resonance signal each, shielded in comparison to the free ligands by 76 ppm for **10** and **12** (acetone-d_6) and 38 ppm for compound **11** (DMSO-d_6).

Even though complexes **13-15** were relatively well soluble in $CDCl_3$, the resonance signals were better resolved in acetone-d_6. **Figure 31** shows the stacked ^{1}H NMR spectra of ligand **4** and complex **13**. With the exception of some overlaps in the case of complexes **13** and **15** where the resonance signal for H_7 overlaps with the resonance signal for CH_2CH_2Se and NCH_2CH_2O, respectively, the signals are well separated.

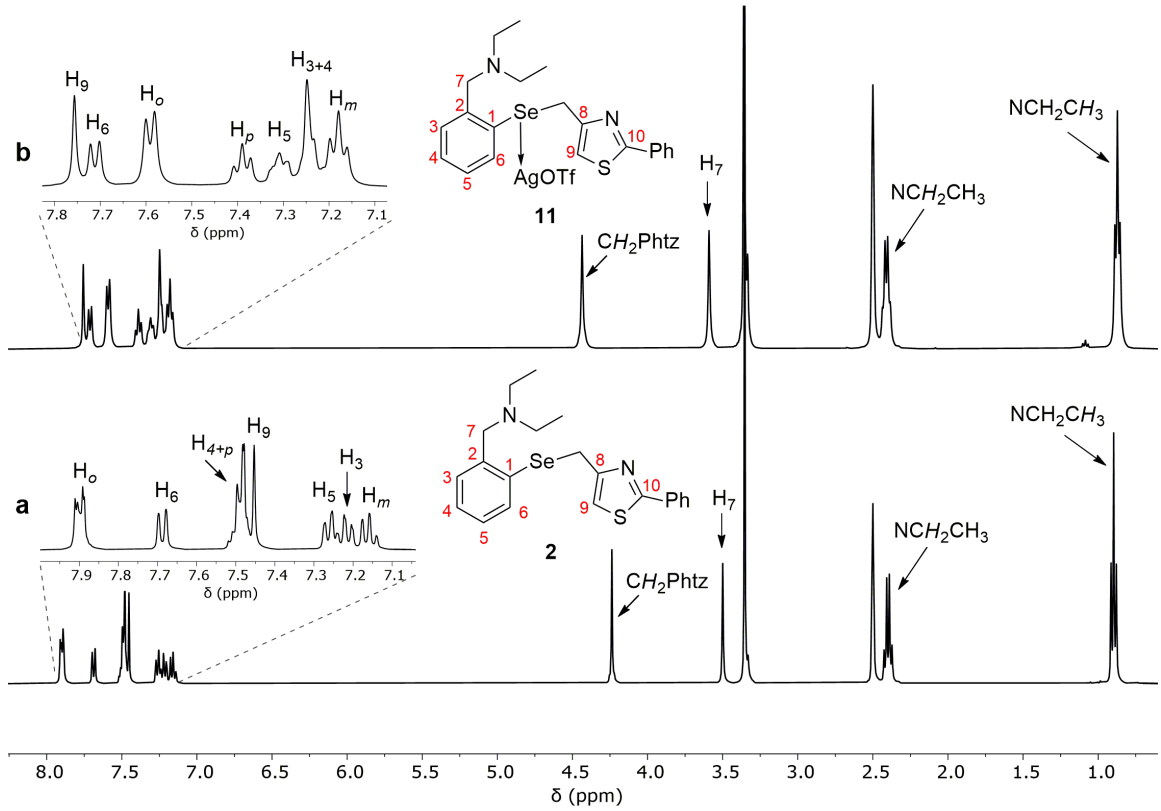

Figure 29. Stacked ^{1}H NMR spectra (DMSO-d_6) of (a) ligand **2** and (b) complex **11**.

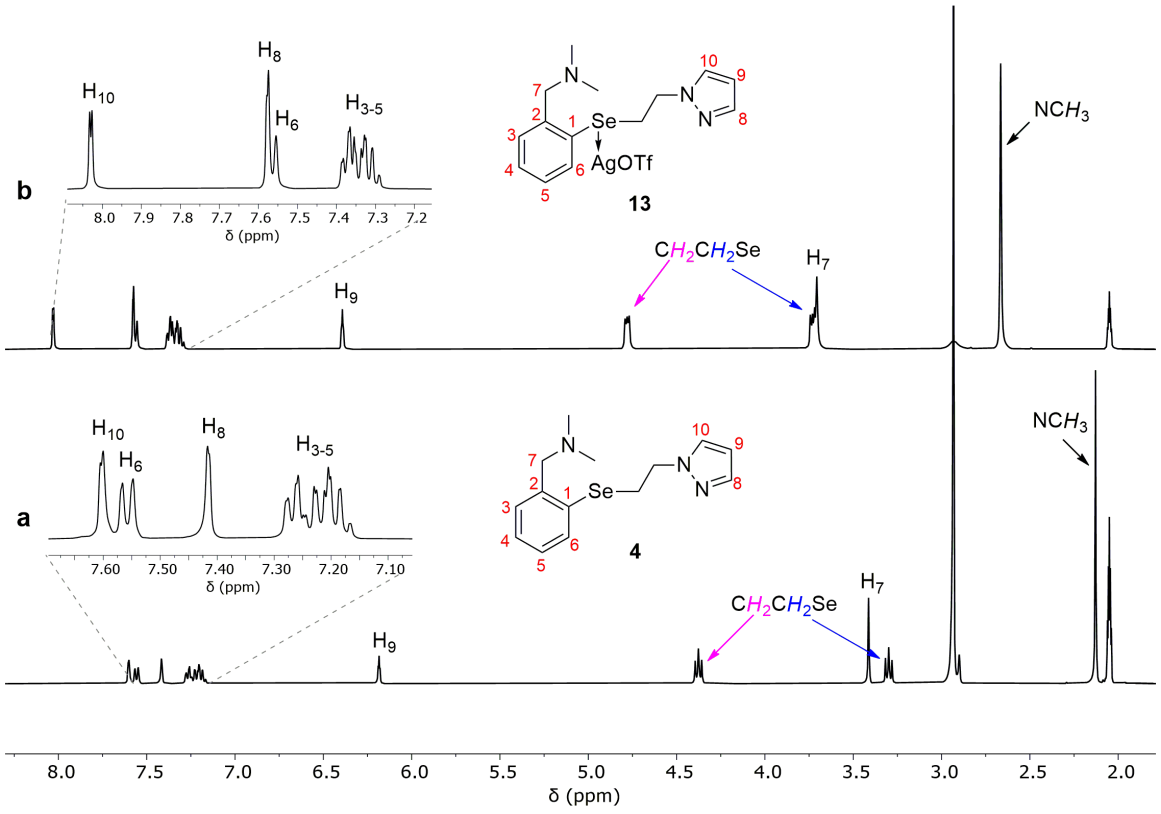

Figure 31. Stacked ^{1}H NMR spectra (acetone-d_6) of (a) ligand **4** and (b) complex **13**.

For compounds **13-15**, the $^{77}Se\{^{1}H\}$ NMR spectra present one resonance signal, shielded in comparison to the free ligands by 22 ppm, indicating the presence of a Se···Ag interaction in solution.

For complex **17**, the ^{1}H NMR spectrum shows similar resonance signals to those of the free ligand, with the aromatic region suffering important changes. The resonances corresponding to H_6 and H_8 are the most affected, indicating the involvement of the nitrogen atom from the pyrazole ring into an interaction. The singlet resonance signal in the $^{77}Se\{^{1}H\}$ NMR spectrum is upfield shifted by 6 ppm in comparison to the ligand's signal.

The $^{13}C\{^{1}H\}$ NMR spectra of all the complexes show all the expected resonance signals and were assigned using 2D NMR spectra. In comparison with the ligands' spectra, the resonance signals are deshielded and an additional low intensity quartet resonance signal is present in all cases. It corresponds to the carbon atom in the CF_3 group around 120 ppm with a coupling constant $^{1}J_{CF}$ of approx. 320 Hz.

The presence of fluorine in the molecules was confirmed by the $^{19}F\{^{1}H\}$ NMR spectra which show a single singlet resonance signal at $\delta_{19F} = -77$ ppm, indicating the ionic behaviour of the triflate group in solution.

Mass spectrometry

The ESI+ mass spectra brought evidence for the complexation of the ligands to the silver centre. The base peaks appear at *m/z* values corresponding to the $[LAg]^+$ fragment in all cases. For example, the ESI+ HRMS spectrum of compound **13** shows peaks at *m/z* values of 415.97945, 308.06609, 265.02393 and 214.01294 corresponding to the $[LAg]^+$, $[L - H]^+$, $[L - NMe_2]^+$ and $[L - CH_2CH_2pz]^+$ fragments, respectively.

Molar conductivity measurements

The molar conductivity measurements for 10^{-3} M solutions in MeCN of compounds **10**-**12** indicate a 1:1 cationic to anionic species electrolyte behaviour.[126,127] The molar conductivity measurements for 10^{-3} M solutions in MeOH of compounds **13**-**15** and **17** indicate a 1:1 electrolyte behaviour as well.[127]

Infrared spectroscopy

All the complexes were investigated in bulk by IR spectroscopy. For complexes **10**-**12**, the characteristic bands for the thiazole ring that appear in the region 1040-1600 cm^{-1} overlap with the bands for the triflate moiety.[128] Some of the strongest bands in the spectra appear in the regions 740-770 cm^{-1} and 630-660 cm^{-1} and correspond to the out-of-plane

vibration of the =C–H bonds in monosubstituted and 1,2-disubstituted benzene rings. In the case of the silver-containing species **13**-**15** and **17**, a series of three bands corresponding to *N*-alkylated pyrazoles were identified in the region 1250-1520 cm^{-1}.[129] Strong bands corresponding to the out-of-plane vibrations of the =C–H bonds in the phenyl ring appear at approx. 750 cm^{-1} and around 630 cm^{-1} for the 1,2-disubstituted benzene rings.

In the spectra of complexes **10**-**15**, four characteristic bands for the triflate moiety were identified.[130] The very strong band centered around 1250 cm^{-1} assigned to the $\nu_{as}(CF_3SO_3)$ moiety in the discussed complexes appears as broad and only slightly splitted band, making the interpretation of the spectra difficult. In addition, the poor splitting of the bands might also indicate a weaker bonding between the metal and the triflato ligand.[130] Thus, the spectra of the complexes indicate the presence of a covalent bonded triflato ligand, which is in agreement with the X-ray diffraction studies for complexes **11** and **12**.

In the case of complex **17**, the C–H stretching bands in the aldehyde (2855 and 2754 cm^{-1}) and the C=O stretching band (1671 cm^{-1}) were also identified. Four strong and very strong bands were identified for the triflate moiety at 1279/1249, 1221/1205, 1158 and 1021 cm^{-1}. The splitted pattern of the bands at 1279/1249 and 1221/1205 cm^{-1} assigned to the asymmetric vibrations of SO_3 and CF_3, respectively, indicate the covalent behaviour of the triflato ligand.[130]

Single-crystal X-ray diffraction studies

The molecular structures of compounds **11** and **12** (**Figure 37**) revealed monomeric species in which the ligands act as *N*,*Se*,*N*-triconnective moieties, with the nitrogen atom from the pendant arm (N1), the nitrogen atom from the thiazole ring (N2) and the selenium atom coordinated to the silver centre in both cases.

For complex **11**, the silver atom is pentacoordinate with two oxygen atoms from the triflate group coordinated, thus resulting into a distorted square pyramidal coordination geometry around the metal centre ($\tau_5 = 0.004$, *vs.* $\tau_5 = 0$ for an ideal square pyramid and $\tau_5 = 1$ for an ideal trigonal bipyramid[132,133]), while in complex **12**, the metal centre is only tetracoordinated with one oxygen atom from the triflate group occupying the fourth coordination position, thus giving rise to a distorted coordination geometry between an ideal tetrahedron and an ideal see-saw ($\tau_4' = 0.62$, *vs.* $\tau_4' = \tau_4 = 0$ for an ideal square planar, $\tau_4' = 0.24$ and $\tau_4 = 0.43$ for a see-saw, and $\tau_4' = \tau_4 = 1$ for an ideal tetrahedral coordination geometry[134,135]).

Due to the strong heteroatom–silver interactions six-membered C_3NAgSe and five-membered C_2NAgSe non-planar chelate rings are formed, which are folded about the Se1···C7 and the Ag1···C12 imaginary axes, respectively. The morpholinyl ring in complex **12** adopts a chair conformation with N1 and O1 in apices. The torsion angle of the phenyl group towards the thiazole ring is 28.04° in complex **11** and 29.04° in complex **12**. The selenium atom has a distorted pseudo tetrahedral coordination geometry in both complexes. Both species present weak intramolecular interactions.

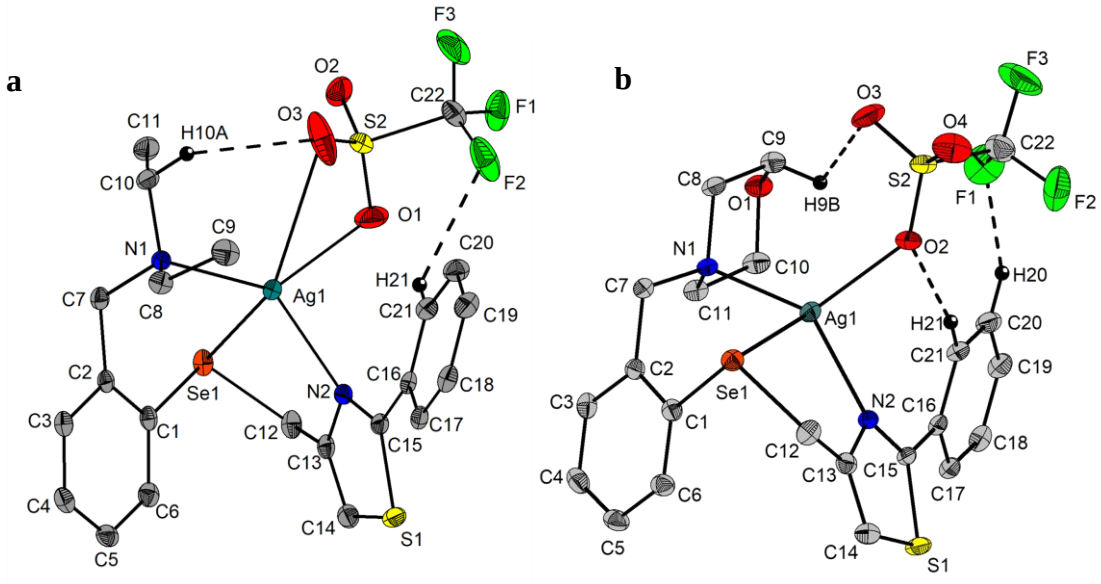

Figure 37. Thermal ellipsoids representation of (a) complex **11** and (b) complex **12** at 50% probability level. Hydrogen atoms that are not involved in intramolecular interactions were omitted for clarity.

The independent molecules of each species are further connected through weak hydrogen interactions, thus generating polymeric chains and the chains are further connected through weak hydrogen contacts giving rise to bidimensional layers.

Upon crystallization of compound **15** from a mixture of $CHCl_3/Et_2O$ (1:3 *v/v*) at low temperature (5°C), hydrolysis took place and the molecular structure of $[Ag(OTf)_2Se\{C_6H_4[CH_2N(H)(CH_2CH_2)_2O]-2\}(CH_2CH_2pz)]_2$ (**15h**) was determined by single-crystal X-ray diffraction. In contrast to the phenylthiazole-derived ligands, the protonated pyrazole-based ligand acts as a bidentate, biconective *N*,*Se*-bridging unit in the silver(I) complex **15h**, giving rise to a dimeric species (**Figure 42**). The silver atom is tetracoordinated with a distorted coordination geometry around the metal centre between an ideal tetrahedron and an ideal see-saw ($\tau_4 = 0.63$ and $\tau_4' = 0.79$), with N3 and Se1′ occupying the axial positions and the oxygen atoms in the equatorial positions. Given that the nitrogen atoms in the pendant arms are protonated, the morpholinyl rings are oriented away from the

silver centres. They display a chair conformation with N1 and O1 in the apices. Two intramolecular hydrogen bonds are present between the hydrogen atom at the nitrogen in the morpholinyl ring and an oxygen atom in the neighbouring triflate group (O7′···H1 1.7848 Å).

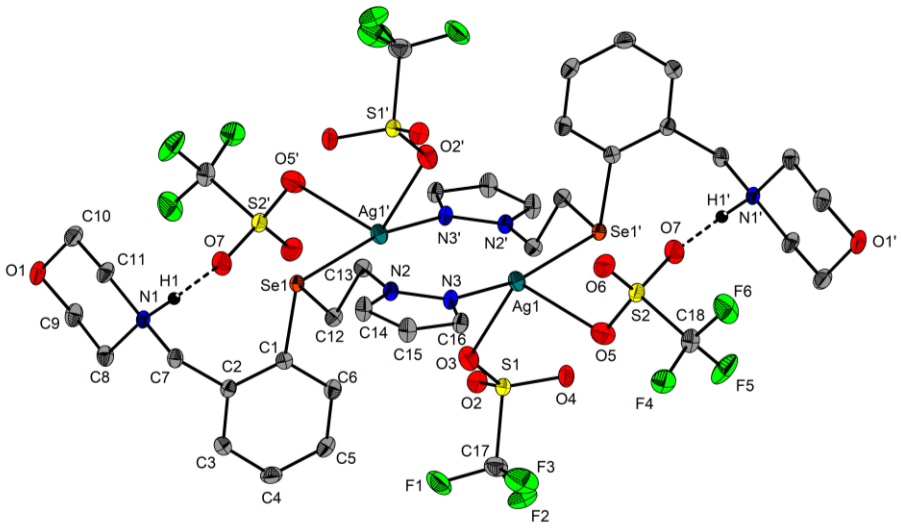

Figure 42. Thermal ellipsoids representation of the dimeric unit in the structure of complex **15h** at 50% probability level. Hydrogen atoms were omitted for clarity, except those involved in intramolecular interactions. Symmetry equivalent atoms (1–x, 1–y, 1–z) are given by "prime".

At the core of the structure lies a 12-membered ring $Ag_2Se_2N_4C_4$ with a non-planar conformation, folded about the two C13···Ag imaginary axes. The two ligand molecules are displayed head-to-tail with the phenyl rings on opposite sides of the 12-membered ring's plane. The N–Ag distances (2.192(2) Å *vs.* Σr_{cov}(Ag,N) = 2.04 Å *vs.* Σr_{vdW}(Ag,N) = 3.25 Å[58]) and Se–Ag distances (2.5306(3) Å *vs.* Σr_{cov}(Ag,Se) = 2.51 Å *vs.* Σr_{vdW}(Ag,Se) = 3.60 Å[58]) suggest strong intramolecular interactions. All four triflate ligands in the dimer are monodentate bonded to the metal centre with slightly different interatomic distances, O3–Ag1 2.502(2) Å and O5–Ag1 2.7002(26) Å (*vs.* Σr_{cov}(Ag,O) = 2.00 Å *vs.* Σr_{vdW}(Ag,O) = 3.10 Å[58]).

III.2.2. Group 11 metal complexes of homoleptic ligand R_2Se

Synthesis

A series of eight metal complexes were obtained by reacting the homoleptic ligand $(pzCH_2CH_2)_2Se$ (**9**) with various silver(I), copper(I) and copper(II) salts in 1:1 molar ratio at room temperature, as depicted in **Scheme 15**.

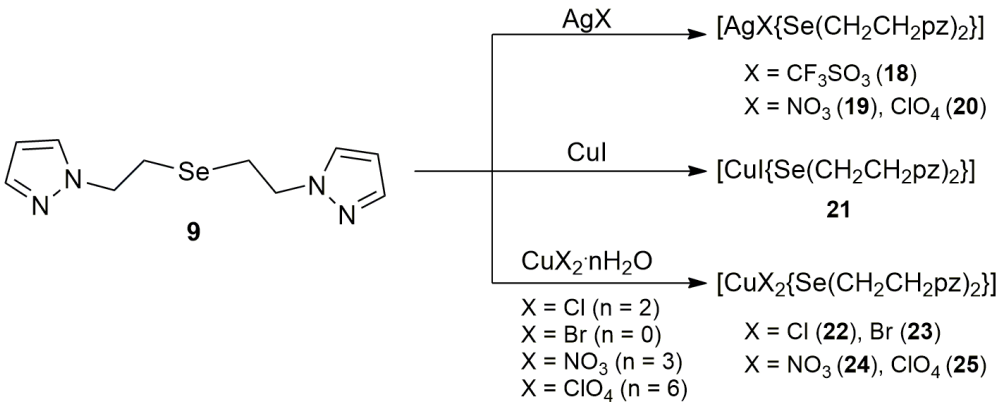

Scheme 15. Synthesis of metal complexes **18**-**25**.

The silver(I) complexes were isolated as colourless air-stable light-sensitive solids, while the copper(I) complex as a yellow air-sensitive solid and the copper(II) complexes as air-stable coloured solids, in moderate to good yields. The copper(II) complexes are well soluble in acetonitrile and DMSO, less soluble in acetone, methanol and ethanol, while the silver(I) complexes are soluble in acetonitrile and DMSO and poorly soluble in other organic solvents.

NMR spectroscopy

Comparing the ^{1}H NMR spectra of the silver(I) complexes with the spectrum of the free ligand (**Figure 44**), a downfield shift is observed for all resonances. The shift of the resonance signals of the protons in the pyrazole rings might indicate the presence of an interaction between the nitrogen atoms and the silver atom. When comparing the ^{1}H NMR spectra of the complexes amongst themselves, no major difference is observed, indicating the ionic behaviour of the complexes in solution.

The $^{13}C\{^{1}H\}$ NMR spectra of the complexes show the same trend as the ^{1}H NMR spectra with a larger shift of the carbon atom CH_2Se compared to the ligand. It is worth mentioning that in the $^{13}C\{^{1}H\}$ NMR spectrum of complex **18**, a low intensity quartet signal corresponding to the CF_3 moiety is visible (δ = 120.68 ppm, $^{1}J_{FC}$ = 321.81 Hz). The presence of fluorine in the molecule is also confirmed by the resonance signal in the $^{19}F\{^{1}H\}$ NMR

spectrum of the compound at δ = – 77.76 ppm, a value that indicates the ionic behaviour of the triflate group in solution.

In the $^{77}Se\{^{1}H\}$ NMR spectra of the complexes one singlet resonance signal was observed with a chemical shift in the range 120-124 ppm, which is in agreement with data found in literature for similar silver(I) complexes, such as [Ag(OTf){Se(CH_2CH_2(3,5-dmpz))$_2$}] (δ = 129.4 ppm)[52]. The resonance signals of the complexes show no significant shift in comparison to the free ligand; therefore, it is safe to assume that a selenium–silver interaction is either very weak or even absent in solution.

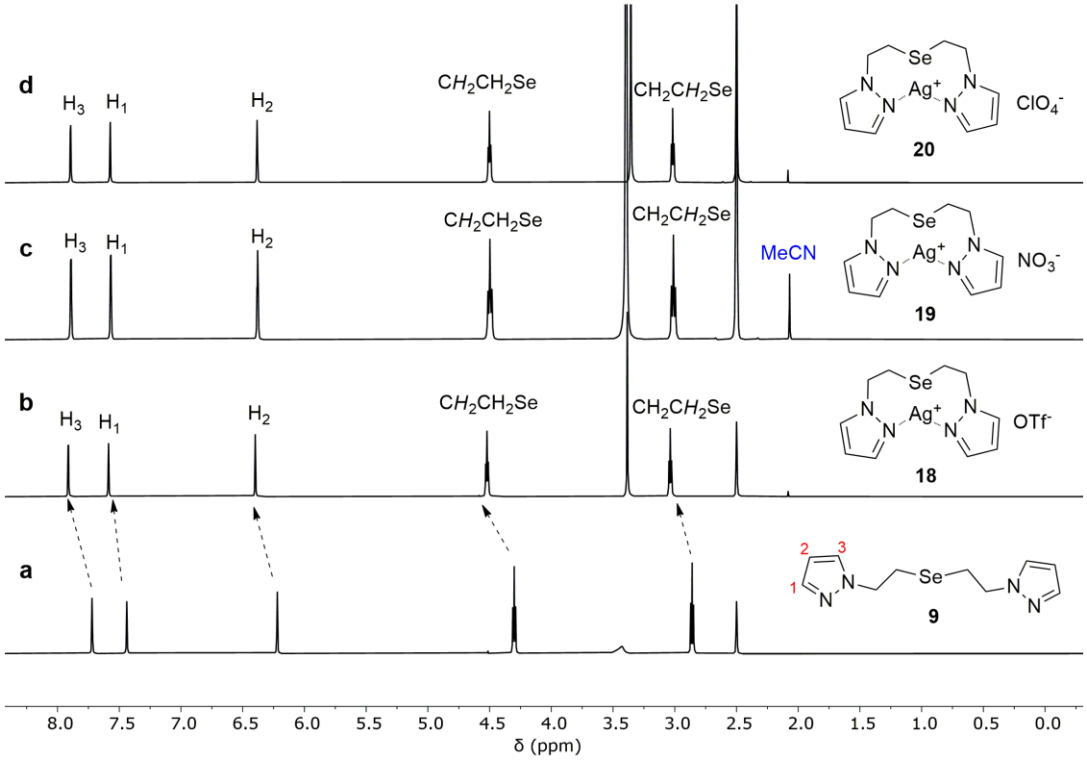

Figure 44. Stacked ^{1}H NMR (DMSO-d_6) spectra of (a) ligand **9**, (b) complex **18**, (c) complex **19** and (d) complex **20**.

The spectra of copper(I) complex **21** indicate the formation of the complex with the resonance signals in the ^{1}H NMR spectrum broader and downfield shifted in comparison to the ligand's resonance signals. The signal in the $^{77}Se\{^{1}H\}$ NMR spectrum of complex **21** is upfield shifted and broadened when compared to the free ligand, indicating the presence of a weak selenium–copper interaction in solution.

Mass spectrometry

The ESI+ mass spectra of these compounds show the base peaks at *m/z* values corresponding to the cations [Ag{Se($CH_2CH_2pz)_2$}]$^+$ (*m/z* = 376.94223) for compounds **18-20,** [Cu{Se($CH_2CH_2pz)_2$}]$^+$ (*m/z* = 332.96600) for complex **21** and [Cu{Se($CH_2CH_2pz)_2$}]$^{2+}$

(*m/z* = 332.96751) for compounds **22-25**. In the spectra of **22** and **24**, respectively, low intensity cations of type $[CuCl\{Se(CH_2CH_2pz)_2\}]^+$ and $[Cu(NO_3)\{Se(CH_2CH_2pz)_2\}]^+$ were also observed.

The ESI– mass spectra of the copper(II) complexes **22-25** show the base peaks corresponding to the $[CuCl_3]^-$, $[CuBr_2]^-$, $[Cu(NO_3)_2]^-$ and $[Cu(ClO_4)_3]^-$ anions at *m/z* = 169.83403, 222.76471, 186.90586 and 361.77187, respectively.

UV-Vis spectroscopy

The UV-Vis spectra of complexes **22-25** recorded for 10^{-3} M solutions in MeOH (**Figure 49**) show strong bands around 229 nm, due to ligand-centered transitions, and weak, broad absorption bands in the region 600-800 nm, due to the *d-d* transitions of d^9 Cu^{2+} cations.[140,141] In the spectra of compounds **22** and **23**, respectively, additional strong bands determined by LMCT transitions appear at 277 and 304 nm, and were assigned to Cl^- and Br^- ligands which remained attached to copper, which was also confirmed by molar conductivity measurements, the compounds behaving as 1:1 electrolytes. These strong absorption bands are not present in the spectra of **24** and **25**, which act as 1:2 electrolytes, as suggested by the values of their molar conductivities.

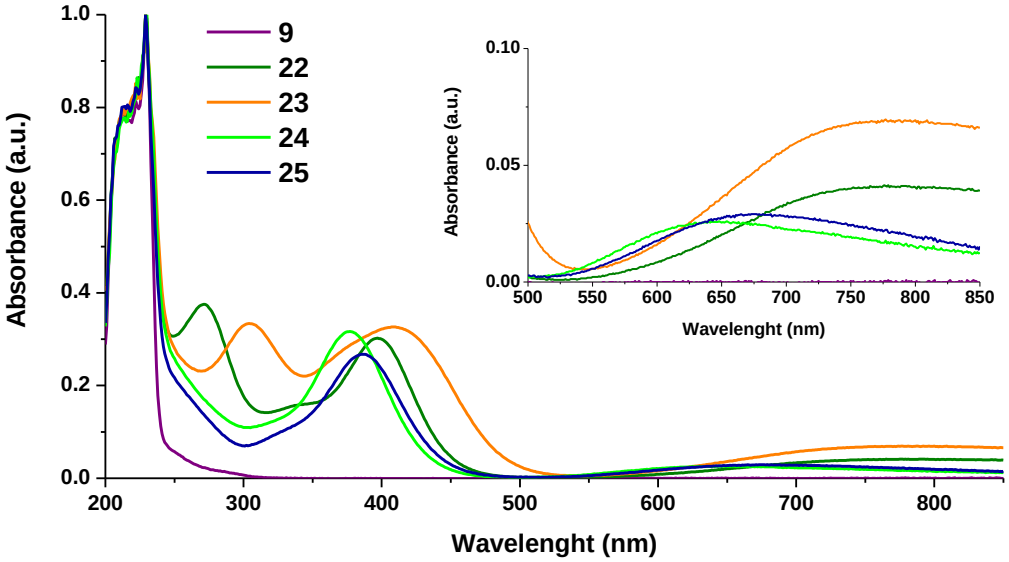

Figure 49. Solution UV-Vis spectra of complexes **22-25** in MeOH (10^{-3} M).

Based on the UV-Vis spectra recorded for MeOH solutions of various ligand to metal molar fractions (constant total concentration 10^{-3} M), Job's method was employed to assign the stoichiometry of the formed species in solution. The absorbance observed around 400 nm was plotted *vs.* the ligand to metal salt molar fraction. The resulting curves with a

maximum at 0.5 correspond to the formation of 1:1 metal to ligand complexes in solution in all four cases (**Figure 50**). The formation of complexes **22**-**25** was also confirmed in solid state by single-crystal X-ray diffraction, as will be further discussed.

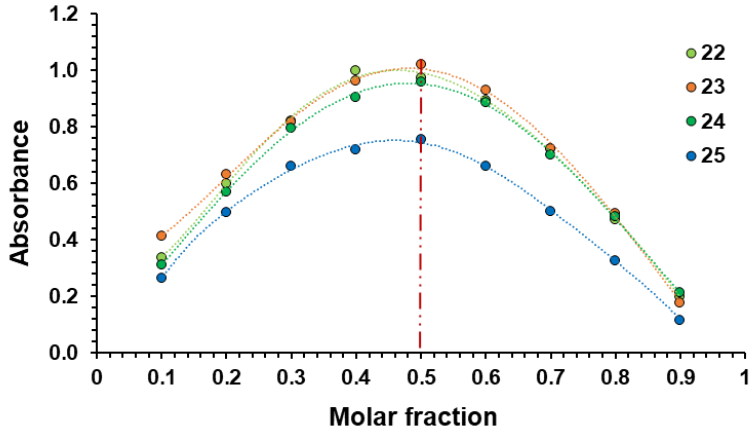

Figure 50. Job's plots for copper complexes obtained by representing the absorbance at λ = 397 nm (**22**), λ = 411 nm (**23**), λ = 377 nm (**24**) and λ = 386 nm (**25**) *vs.* the molar fraction.

When looking at the solid-state UV-Vis spectra of compounds **22**-**25** (**Figure 51**), the bands around 400 nm appear red shifted in all cases, while the characteristic bands assigned to *d*-*d* transitions are very broad and red shifted for halides **22** and **23** and broad and blue shifted for complexes **24** and **25**, when compared with the solution spectra of the compounds. In all cases, the diorganoselenide ligand **9** seems to have a lower denticity in solution than in solid state and this behaviour resulted in the red shift of the band around 400 nm.

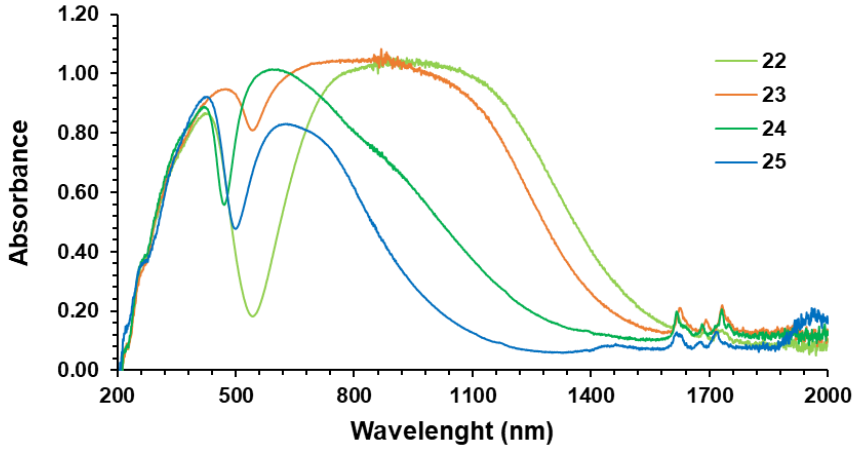

Figure 51. Solid-state UV-Vis spectra of complexes **22**-**25**.

Conductivity measurements were performed for the copper(II) complexes in MeOH solutions (10^{-3} M) at room temperature. The values found for complexes **22**–**25** are in the

characteristic range for either 1:1 or 1:2 electrolytes in MeOH solutions.[126,127] The molar conductivities of these compounds, together with solution and solid-state UV-Vis data, are given in **Table 18**.

Table 18. Molar conductivities and UV-Vis data of the copper(II) complexes **22-25**.

Compound	Λ_M[a] ($\Omega^{-1}\cdot cm^2\cdot mol^{-1}$)	λ_{max}[a] (nm)	λ_{max}[b] (nm)
22	101.40	277; 397; 775	423; 922
23	110.47	304; 411; 763	476; 837
24	171.33	377; 688	420; 592
25	188.26	386; 708	427; 631

[a] 10^{-3} M MeOH solutions; [b] solid state

IR spectroscopy

In the IR spectra of all the compounds a series of three bands in the region 1250-1520 cm^{-1} corresponding to *N*-alkylated pyrazoles were identified.[129] The strongest band in the spectra corresponding to out-of-plane vibration of C–H bonds appears at approx. 760-780 cm^{-1}. For complex **18** the presence of four distinct non-split bands assigned to the $\nu_{asym}(SO_3)$, $\nu_{asym}(CF_3)$, $\nu_{sym}(SO_3)$, $\nu_{sym}(CF_3)$ indicates the ionic behaviour of the triflate moiety.[130] The characteristic bands for unidentate coordinated nitrate groups were identified in the spectra of complex **19** at 1278, 1310, 1340 and 1090 cm^{-1}. The IR spectra of complex **24** indicates the presence of both unidentate and bidentate chelating nitrato groups, in the form of strong and very strong bands at 1410, 1306, 1008 cm^{-1} and 1476, 1275, 1034 cm^{-1}, respectively.[142] For complexes **25** and **20**, strong, broad bands, split in two components at 1092/1064 cm^{-1} and 1094/1062 cm^{-1}, respectively, indicate the presence of coordinated perchlorato ligands in solid state.[142,143]

X-ray diffraction studies

In the case of the silver(I) complexes **18** and **20**, the diorganoselenium ligand behaves as a bimetallic tetraconnective unit acting as a 2 x *N,Se*-chelating moiety between two neighbour silver atoms, giving rise to polymeric chains, with the pyrazole rings of the ligand units alternating on opposite sides of the plane containing the silver atoms in the –Ag–Se–Ag–Se–Ag–Se– zig-zag skeleton. As a result, the silver atom becomes tetracoordinate.

In the unit cell of compound **18**, four independent anion-cation pairs are present (**18a-18d**). **Figure 53** shows the thermal ellipsoids representation of a chain built of four independent cations in **18**. In contrast, in the unit cell of complex **20**, the repeating unit consists of only one type of molecule.

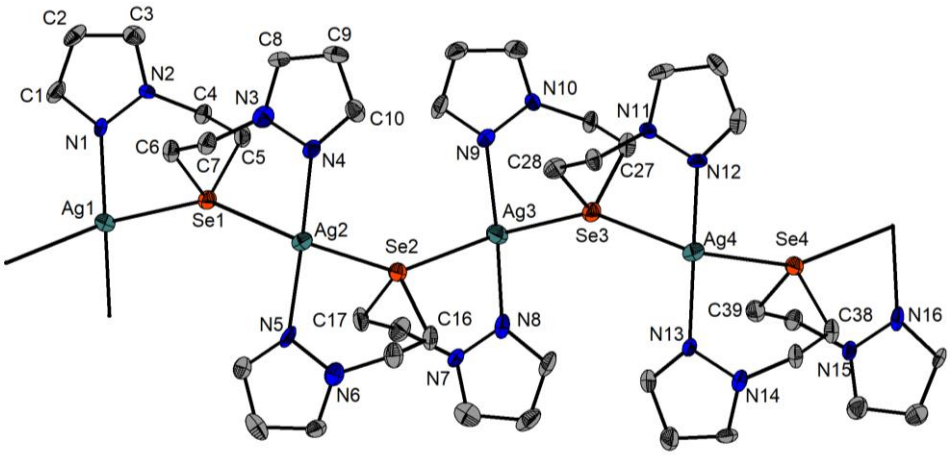

Figure 53. View along *c* axis of thermal ellipsoids representation of a chain of $[AgSe(CH_2CH_2pz)_2]^+$ cations from the four independent molecules in complex **18**, at 50% probability level.

In both cases, the silver and selenium atoms present a distorted see-saw coordination geometry. The Se–Ag interatomic distances in the polynuclear chains have similar magnitudes, between 2.80 and 2.90 Å (*vs.* Σr_{cov}(Ag,Se) = 2.51 Å and Σr_{vdW}(Ag,Se) = 3.70 Å[58]). The bond lengths Ag–N (2.189(12)-2.234(12) Å in **18** and 2.187(5)-2.198(6) Å in **20**) and Ag–Se (2.819(2)-2.905(2) Å in **18** and 2.8562(8)-2.9049(8) Å in **20**) are in the range found for other silver(I) complexes with functionalized pyrazole-based ligands.[66,144] The formed six-membered AgN_2C_2Se chelate rings have twisted boat conformations with silver and one of the carbon atoms in apices. The parallel chains of cations in the crystals of **18** and **20** are joined in a 3D supramolecular network by weak cation-anion interactions.

Complexes **22**, **22**·MeOH and **23** crystallize in the orthorhombic space group $P2_12_12_1$, monoclinic space group P21/c and monoclinic C c space group, respectively, and have very similar solid-state structures (**Figure 56**) with the penta-coordinated copper(II) in a distorted trigonal bipyramidal coordination geometry with the two halogen atoms and selenium in equatorial positions and the two pyrazole nitrogen atoms in apical positions. The interatomic distance between Se and Cu, 2.6477(9) Å in **22**, 2.5695(3) Å in **22**·MeOH and 2.5355(5) Å in **23**, indicates a strong Se–Cu interaction (Σr_{vdW}(Cu,Se) = 3.40 Å *vs.* Σr_{cov}(Cu,Se) = 2.34 Å[58]).

The two slightly different Cu–X interatomic distances (X = Cl in **22** and Br in **23**) with values closer to the sum of the covalent radii of the two elements (Σr_{cov}(Cu,Cl) = 2.16 Å, Σr_{vdW}(Cu,Cl) = 3.21 Å, Σr_{cov}(Cu,Br) = 2.21 Å, Σr_{vdW}(Cu,Br) = 3.35 Å[58]), suggest a covalent structure in solid state for these species.

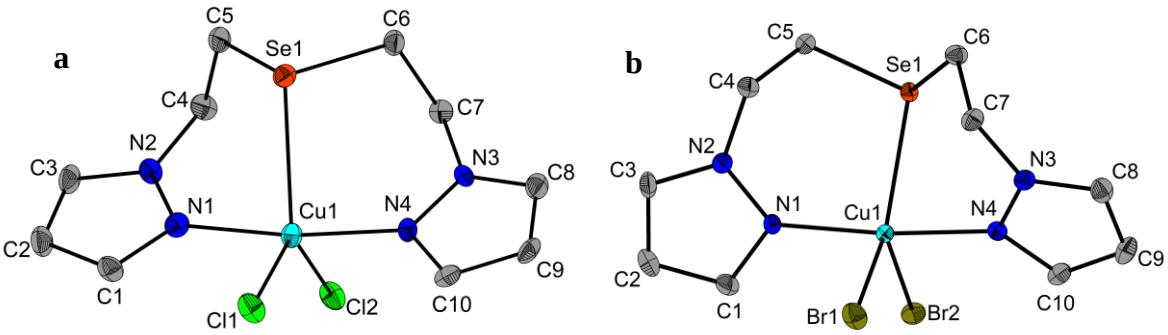

Figure 56. ORTEP diagram of (a) complex **22** and (b) complex **23** with ellipsoids at the 50% probability level. Hydrogen atoms were omitted for clarity.

In the crystal packing of compounds **22** and **23**, weak intermolecular X···H bonding (X = Cl in **22** and Br in **23**) between each of the two halogen atoms and hydrogen atoms belonging to neighbour molecules were evidenced. Polymeric chains are formed *via* short contacts between Cl1 in **22** and Br2 in **23** and hydrogen atoms in the $–CH_2CH_2–$ fragment as shown in **Figure 58** and **Figure 59**, respectively.

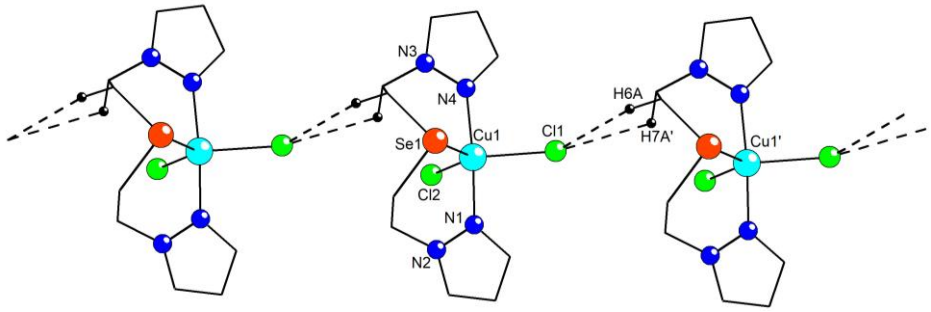

Figure 58. Best view of polymeric chain in the crystal of **22**. Hydrogen atoms, except those involved in intermolecular interactions, are omitted for clarity. Symmetry equivalent positions (1+x, y, z) are given by "prime".

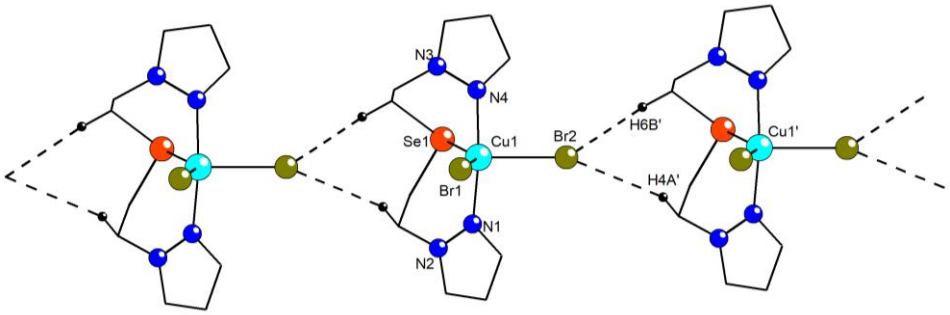

Figure 59. Best view of the polymeric chain in the crystal of **23**. Hydrogen atoms, except those involved in intermolecular interactions, are omitted for clarity. Symmetry equivalent positions (1/2+x, –1/2+y, z) are given by "prime".

These chains are further connected through X···H contacts generating 2D layers, which are finally connected by short X···H contacts in 3D supramolecular networks.

In complexes **24** and **25**·H_2O, the metal centre is hexa-coordinated with a distorted octahedral coordination geometry (**Figure 60**). In **24**, the two nitrato groups act differently, one of them coordinates bidentate through two oxygen atoms (O1–Cu1 2.030(11) Å and O2–Cu1 2.563 Å *vs.* Σr_{cov}(Cu,O) = 1.83 Å and Σr_{vdW}(Cu,O) = 2.80 Å[58]), while the other coordinates through only one oxygen atom (O4–Cu1 2.254(11) Å). In contrast with this behaviour, in **25**·H_2O both perchlorato groups act as monodentate ligands, through weak O···Cu interactions (O2···Cu1 2.55 Å, O6···Cu1 2.65 Å, *vs.* Σr_{cov}(Cu,O) = 1.83 Å and Σr_{vdW}(Cu,O) = 2.80 Å[58]). The octahedral coordination sphere of copper in **25** is completed by a water molecule (H_2O···Cu 2.015 Å).

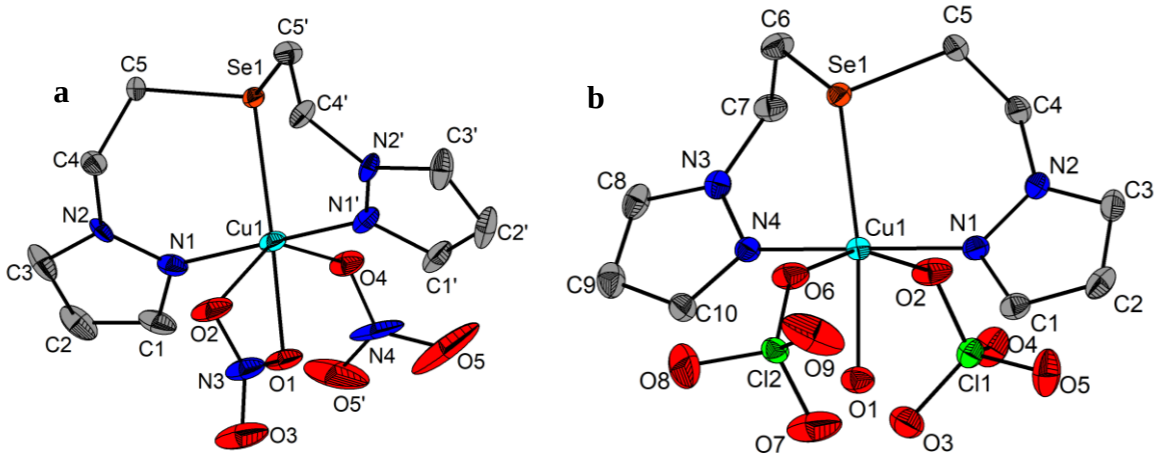

Figure 60. ORTEP diagram of (a) complex **24** with ellipsoids at the 40% probability level and (b) complex **25**·H_2O with ellipsoids at the 50% probability level. Hydrogen atoms were omitted for clarity.

In the crystals of **24** and **25**·H_2O, polymeric chains are formed *via* weak O···H intermolecular contacts between oxygen atoms in the anionic ligands and hydrogen atoms in the –CH_2CH_2– fragments in **24** (O1″···H5B/H5B′ 2.34 Å) or in the pyrazole ring (O9···H8′ 2.48 Å) in **25**·H_2O (**Figure 61** and **Figure 62**). These chains are further connected in 2D layers through O···H intermolecular interactions. Finally, the 2D layers are connected in 3D supramolecular architectures by very weak O···H contacts of 2.58 Å.

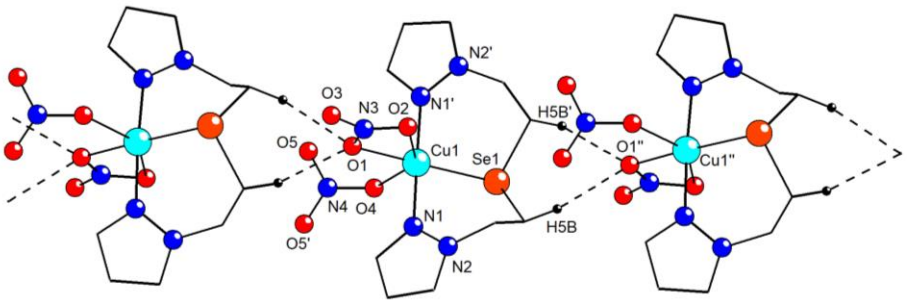

Figure 61. Best view of polymeric chains in the crystal of **24**. Hydrogen atoms that are not involved in intermolecular interactions, are omitted for clarity. Symmetry equivalent positions (x, 3/2–y, z) and (–1/2+x, 3/2–y, 3/2–z) are given by "prime" and "double prime", respectively.

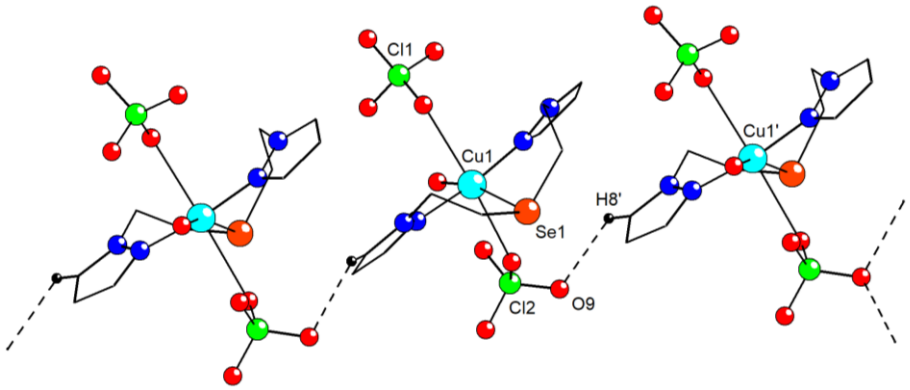

Figure 62. Best view of a polymeric chains in the crystal of **25**·H_2O. Hydrogen atoms, except those involved in intermolecular interactions, are omitted for clarity. Symmetry equivalent positions (1/2+x, 3/2–y, 1/2+z) are given by "prime".

III.2.3. Evaluation of antiproliferative activity

Silver(I) complexes **10**-**12**, **15**, **18** and **20** were screened for antiproliferative activity on murine melanoma B16.F10 cells and proved to have similar activity against this type of cells, while showing an increase in the activity compared to the corresponding free ligands **1**-**3**, **6** and **9**, respectively (See section **III.1.3**). **Figure 63** presents the effects of various concentrations of the compounds on cancer cell proliferation and **Table 23** shows the calculated IC_{50} values.

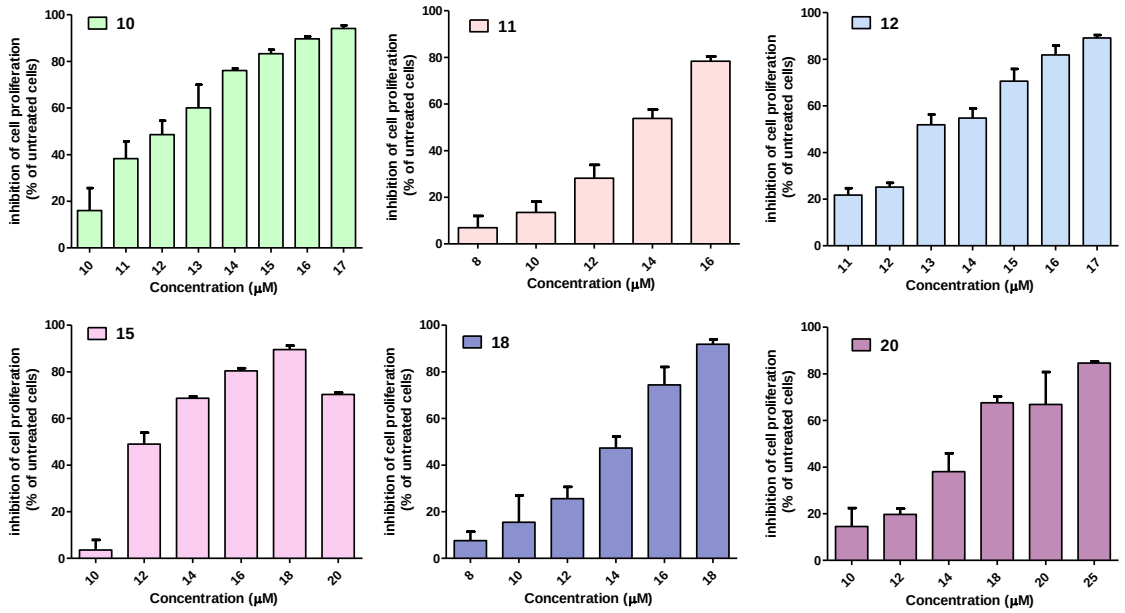

Figure 63. Concentration-dependent antiproliferative effect of compounds **10**-**12**, **15**, **18** and **20** in comparison with untreated control B16.F10 cells.

Table 23. IC_{50} values of compounds **10**-**12**, **15**, **18**, **20**, silver(I) salts and the standard drug Dacarbazine.

Compound	IC_{50} (µM)	Compound	IC_{50} (µM)
10	11.84	**18**	14.42
11	15.91	**20**	15.78
12	14.24	**AgOTf**	29.34
15	11.11	**$AgClO_4$**	33.79
Dacarbazine[124]	149.7		

The obtained results are in the same range to those reported for a series of $AgNO_3$ complexes of pyridine and (benz)imidazole derivatives on murine melanoma B16 cells (IC_{50} = 2.44 to 28.65 µM *vs.* $AgNO_3$ IC_{50} = 9.74 µM, determined by MTT assay)[150] and higher than for silver(I) complexes with 2-benzoylpyridine-derived hydrazones on murine melanoma B16.F10 cells (IC_{50} = 2.00 to 2.36 µM, *vs.* $AgNO_3$ IC_{50} = 75.40 µM, determined by MTT assay).[151] In both cases, complexation of the ligands with silver(I) nitrate increased the activity and selectivity.

III.3. Metal complexes with organoselenolato ligands

A literature study revealed that diorganotin(IV) bis(organoselenolates) are not a very common presence. Compounds containing pyridyl[158–160] or pyrimidyl[161] groups, methyl, phenyl or benzoyl[162] groups attached to the selenium atom were synthesized and structurally characterized by appropriate methods. They were largely synthesized by two methods: (*i*) oxidative addition of diorganodiselenides to Sn(II) species[168] and (*ii*) reaction of metal organoselenolates with diorganotin(IV) dihalogenides,[161] the latter being used in this work as well.

III.3.1. Synthesis and structural characterization

Synthesis

The diorganodiselenide, $(pzCH_2CH_2)_2Se_2$ (**26**), was synthesized following a literature method,[105] by reacting 1-(2-bromoethyl)-1*H*-pyrazole with freshly prepared Na_2Se_2 in absolute ethanol under reflux. A series of tin(IV) bis(organoselenolates) were obtained by cleavage of the Se–Se bond in diorganodiselenide **26** with $NaBH_4$ in degassed absolute ethanol at 0°C, followed by the reaction of the resulting sodium organoselenolate with the corresponding diorganotin dichloride in a 2:1 molar ratio as depicted in **Scheme 17**. Only compound **30** was obtained as a solid, the other tin(IV) derivatives being isolated as colourless oils.

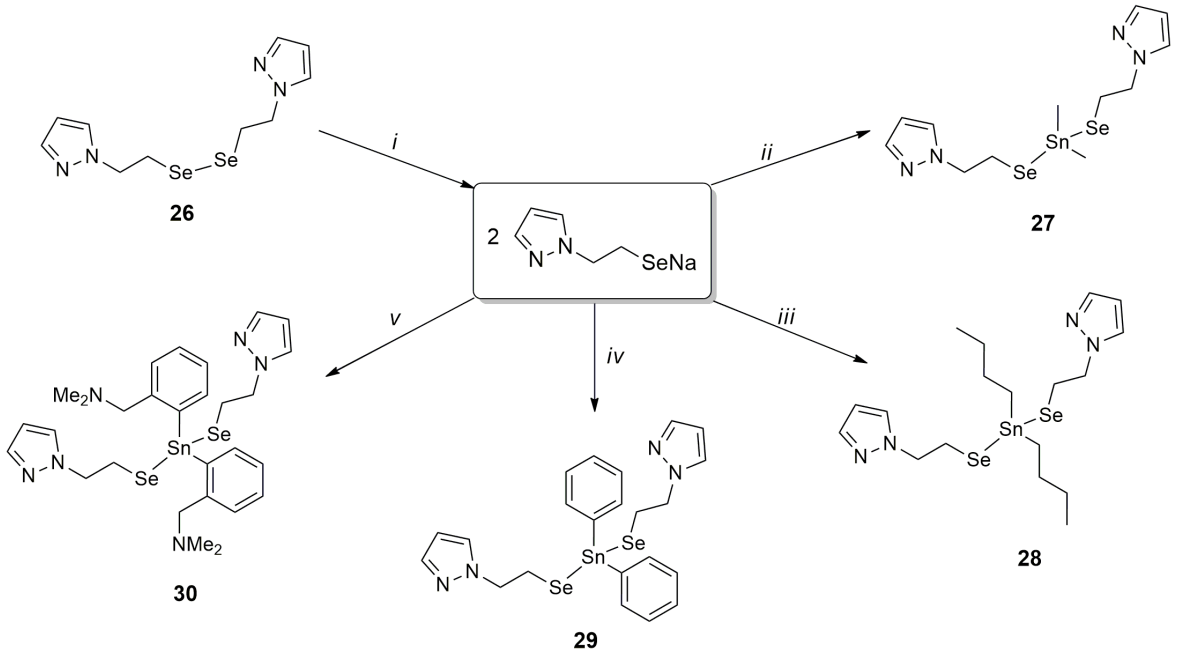

Scheme 17. Synthetic pathway for preparation of tin(IV) bis(organoselenolates) **27**-**30**. Reagents and reaction conditions: *i)* $NaBH_4$, degassed absolute EtOH, 0°C; *ii)* Me_2SnCl_2; *iii*) Bu_2SnCl_2; *iv*) Ph_2SnCl_2; *v*) $[2\text{-}(Me_2NCH_2)C_6H_4]_2SnCl_2$.

NMR spectroscopy

In the ^{1}H NMR spectra of compounds **27-30**, two triplet resonance signals corresponding to the ethylene moieties, a triplet and two doublet resonance signals for the pyrazole ring represent the resonance signals for the common groups in all compounds (**Figure 64**). In the aliphatic region, the resonance signal corresponding to the CH_2SeSn moiety is accompanied by tin satellites with $^{3}J_{119SnH}$ of 28-40 Hz. In addition, for compound **27** a sharp singlet resonance signal for the methyl groups accompanied by tin satellites can be observed, while for compound **28**, a triplet and three multiplet signals corresponding to the butyl moieties are present. In compound **29** additional resonance signals corresponding to the phenyl moieties appear in the aromatic region.

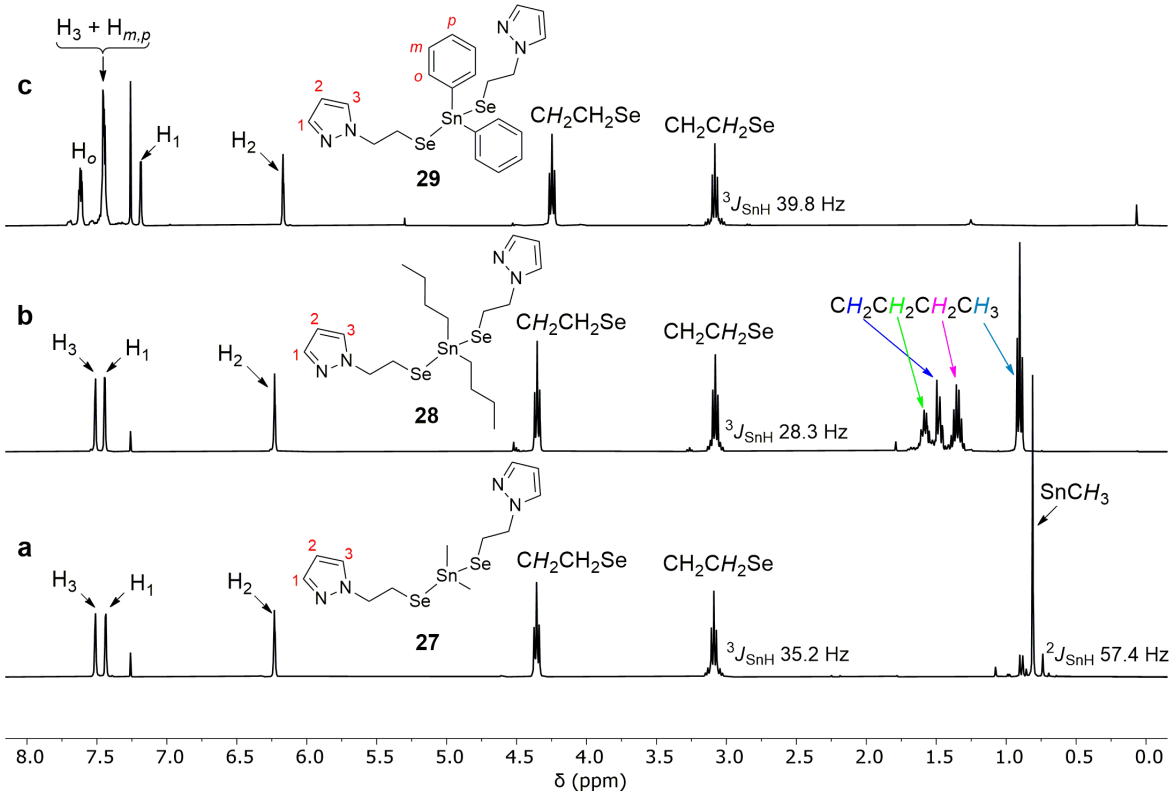

Figure 64. Stacked ^{1}H NMR spectra ($CDCl_3$) of (a) compound **27**, (b) compound **28** and (c) compound **29**.

In the ^{1}H NMR spectrum of compound **30** all the signals were assigned with the help of 2D NMR spectra. In contrast to the starting material [2-(Me_2NCH_2)C_6H_4]$_2SnCl_2$ which shows intramolecular N···Sn interaction in solution at room temperature (AB spin system for protons H_7 and broad resonance signal for CH_3 groups), compound **30** does not show such a behaviour in solution at room temperature, the 12 equivalent methyl protons of the pendant arms giving a sharp singlet resonance signal and the CH_2 groups giving a very broad resonance signal (**Figure 65**), indicating a dynamic behaviour in solution, based on the

decoordination, inversion at nitrogen and recoordination of the nitrogen atom to tin, as was first observed by Iwaoka.[55]

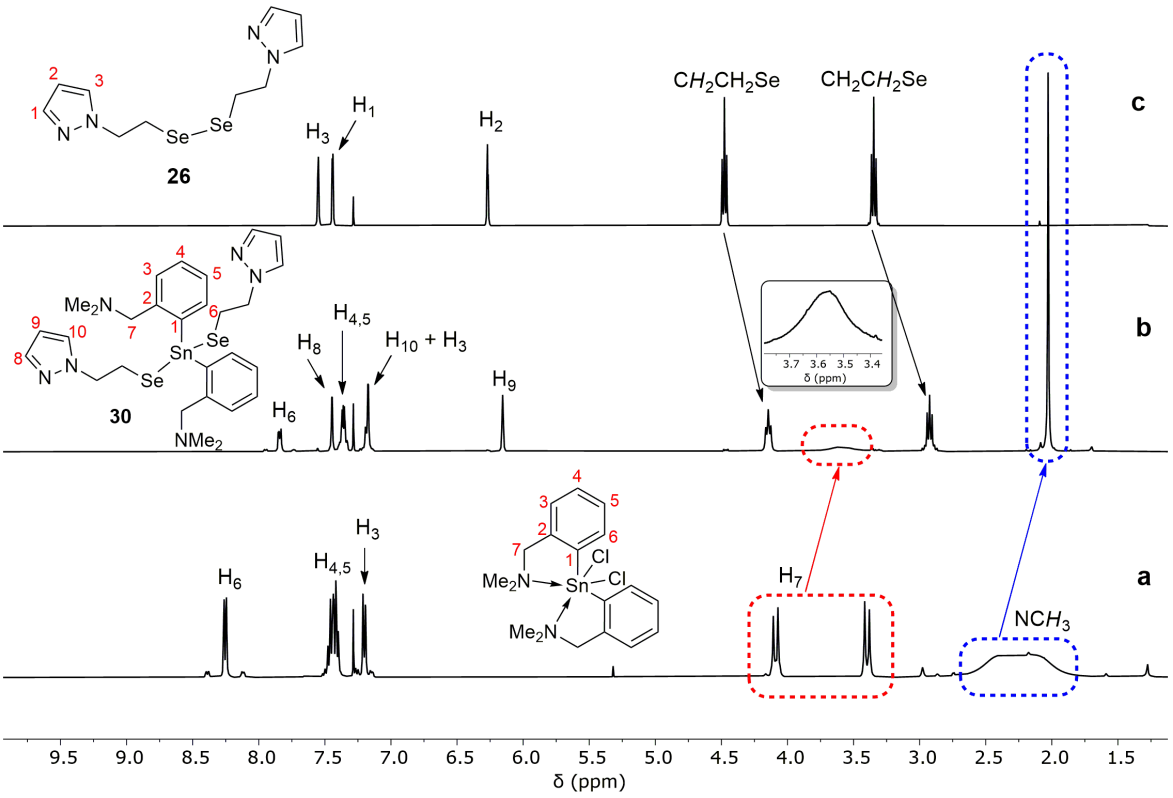

Figure 65. Stacked ^{1}H NMR spectra ($CDCl_3$) of (a) $[2\text{-}(Me_2NCH_2)C_6H_4]_2SnCl_2$, (b) compound **30** and (c) diorganodiselenide **26**.

The resonance signals in the $^{13}C\{^{1}H\}$ NMR spectra confirm the identity of the compounds. In most cases, the signal-to-noise ratio was sufficiently low for the observation of ^{77}Se and/or $^{117/119}$Sn satellites corresponding to $^{1}J_{SeC}$ and $^{n}J_{117/119SnC}$ (n = 1-4), respectively.

The $^{77}Se\{^{1}H\}$ and $^{119}Sn\{^{1}H\}$ NMR chemical shifts for all the compounds and starting materials measured at room temperature in $CDCl_3$ are summarized in **Table 25**. The $^{77}Se\{^{1}H\}$ NMR spectra of all compounds displayed singlet resonance signals (range –146 to –183 ppm) which are flanked by $^{117/119}$Sn satellites with $^{1}J_{117/119SnSe}$ coupling constants in the range of 1030–1320 Hz.

The $^{119}Sn\{^{1}H\}$ NMR spectra of all compounds displayed a single resonance signal confirming the existence of only one tin(IV) species in solution. The resonances appeared in the range of 80 to –136 ppm. In all the cases the resonance signals were accompanied by ^{77}Se satellites with the $^{1}J_{119SnSe}$ coupling constant values between 1057 and 1320 Hz. **Figure 67** shows the resonance signals in the $^{77}Se\{^{1}H\}$ and $^{119}Sn\{^{1}H\}$ NMR spectra of compound **27**, accompanied by $^{117/119}$Sn and ^{77}Se satellites, respectively.

Table 25. Centralized NMR data for compounds **26-30** and diorganotin(IV) dichlorides used as starting materials.

Compound	δ_{77Se} (ppm)	$^1J_{SeSn}$ (Hz)	δ_{119Sn} (ppm)	$^1J_{119SnSe}$ (Hz)	Starting material	δ_{119Sn} (ppm)
26	283.0	-	-	-	-	-
27	– 146.0	1152.5 (^{117}Sn) 1209.2 (^{119}Sn)	58.2	1209.8	Me_2SnCl_2	143.7
28	– 177.7	1181.7 (^{117}Sn) 1236.7 (^{119}Sn)	79.9	1231.9	Bu_2SnCl_2	128.6
29	– 182.3	1261.7 (^{117}Sn) 1319.2 (^{119}Sn)	– 23.5	1319.3	Ph_2SnCl_2	– 27.2
30	– 181.0	1039.9 (^{119}Sn)	– 136.0	1057.5	R_2SnCl_2	– 254.1

R = [2-(Me_2NCH_2)C_6H_4]

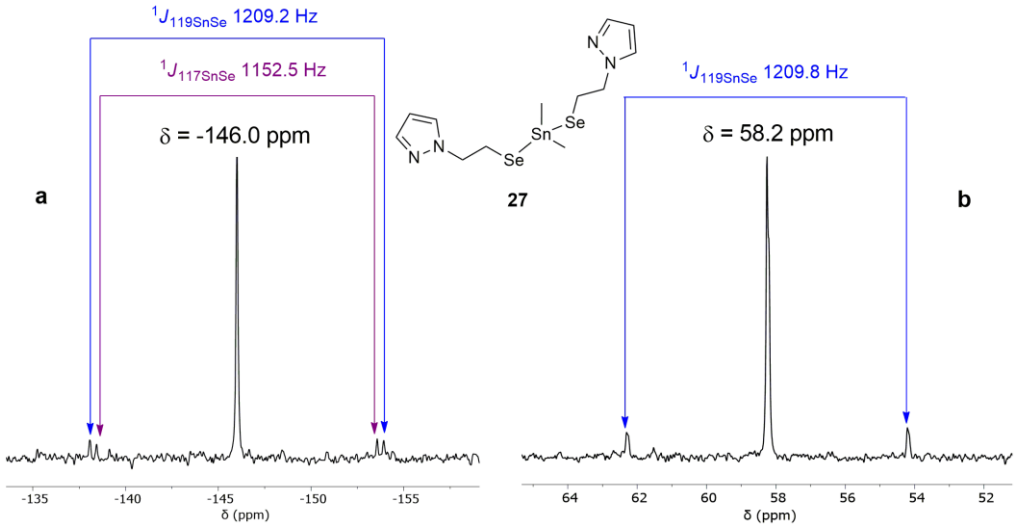

Figure 67. (a) $^{77}Se\{^1H\}$ NMR spectrum ($CDCl_3$) and (b) $^{119}Sn\{^1H\}$ NMR spectrum ($CDCl_3$) of compound **27**.

Based on published studies concerning Me_2Sn, Bu_2Sn and Ph_2Sn derivatives, using the $^2J_{119SnH}$ or $^1J_{119SnC}$ coupling constants' values, we could calculate the C–Sn–C angle in solution ($CDCl_3$).[172–175] For all three derivatives the results indicate a distorted tetrahedral geometry around the tin atom in solution with a C–Sn–C angle between 108 and 111° (**Table 26**).

Table 26. Values of $^2J_{119SnH}$ and $^1J_{119SnC}$ coupling constants and calculated C–Sn–C angles in solution for compounds **27-29**.

Compound	^{1}H NMR		$^{13}C\{^1H\}$ NMR	
	$^2J(^{119}Sn,^1H)$	C–Sn–C	$^1J(^{119}Sn,^{13}C)$	C–Sn–C
27	57.40 Hz	110.7° [172]	361.70 Hz	108.5° [173]
28	-	-	342.27 Hz	108.9° [174]
29	-	-	551.60 Hz	110.0° [175]

$\theta = 0.0161|^2J|^2 - 1.32|^2J| + 133.4$ [172]; $^1J = 11.4\theta - 875$ [173]
$^1J = 9.99\theta - 746$ [174]; $^1J = 15.56\theta - 1160$ [175]

Mass spectrometry

For the discussed organotin(IV) derivatives, a similar behaviour was observed, as the compounds lose a $pzCH_2CH_2Se-$ fragment upon ionization. For example, in the APCI+ HRMS spectrum of compound **28** the identified peaks at *m/z* values 409.02205, 292.88028 and 174.97739, correspond to the $[M - SeCH_2CH_2pz]^+$, $[pzCH_2CH_2SeSn]^+$ and $[pzCH_2CH_2Se]^+$ fragments, respectively.

III.3.2. Evaluation of antiproliferative activity

The diorganodiselenide **26** and the corresponding tin(IV) compounds **27** and **30** were screened for antiproliferative activity against the mouse colon carcinoma C26 cell line using the ELISA-BrdU colorimetric assay. The effects of various concentrations of the compounds on cancer cell proliferation are presented in **Figure 69**. The cytotoxic actions of the compounds on C26 cells were similar and correlated positively with the concentrations tested (r = 0.96 for **26**; r = 0.93 for **27**; r = 0.98 for **30**). Our finding was also supported by calculation of IC_{50} values for these compounds (**Table 27**).

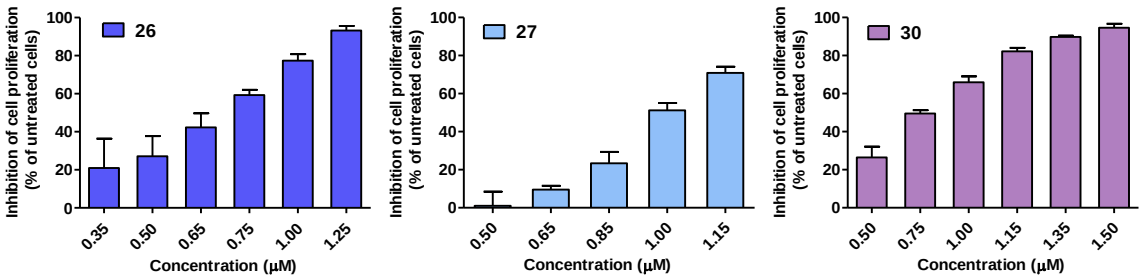

Figure 69. Concentration-dependent antiproliferative effect of compounds **26**, **27** and **30** in comparison with untreated control cells.

Table 27. IC_{50} values of compounds **26**, **27**, **30** and standard drugs.

Compound	**27**	**28**	**31**	5-fluorouracil	Deltonin
IC_{50} (μM)	0.77	0.92	0.94	5.38	1.22

The obtained values suggest that the presence of tin does not bring any significant contribution for enhanced antiproliferative activity. However, these values represent a significantly increased activity in comparison with the currently used compounds in chemotherapy for this cell line, *e.g.* 5-fluorouracil (IC_{50} = 5.38 μM) or other tested compounds, such as the steroidal Deltonin (IC_{50} = 1.22 μM).[125]

V. CONCLUSIONS

The present work has brought contributions to the chemistry of azole-containing diorganoselenium compounds and their coordination behaviour towards group 11 metals. Diorganotin(IV) complexes with organoselenolato ligands bearing alkyl groups with pyrazole functionalities were also described. Insights into the stability/reactivity and the specific biological activity of the reported species are reported as well.

The data presented in **Subchapter III.1** shows that the synthesis of heteroleptic diorganoselenides **2** and **4-6** proceeded with higher yields when sodium organoselenolates were used, compared with the procedure based on lithium organoselenolate. All the presented compounds were appropriately characterized, and their antioxidant or antiproliferative activities were investigated.

Compounds **4-9** proved to be moderate antioxidant agents, with compounds **4** and **5** having the best activity as shown by the T_{50} value and confirmed by cyclic voltammetry measurements. The NMR investigation of the reaction mechanism showed that the reactions occur *via* a diorganoselenoxide intermediate which is stabilized by N···Se intramolecular interactions, as confirmed by DFT calculations. The chiral nature of the generated intermediates was observed in the recorded ^{1}H NMR spectra. ^{77}Se NMR spectroscopy proved to be a very useful tool in the investigation of the reaction mechanism.

Phenylthiazole derivatives **1** and **2** have moderate to good antiproliferative activity against murine melanoma B16.F10 cells, while the pyrazole-derivatives **4-6** proved to be inactive against murine colon carcinoma C26 cells.

Subchapter III.2 focused on the investigation of the coordination behaviour of derivatives **1-9** in reaction with various silver(I), copper(I) and copper(II) salts, leading to the isolation of 15 new metal complexes which were structurally characterized both in solution and solid state by using appropriate methods.

The ^{1}H, ^{13}C{^{1}H} and ^{77}Se{^{1}H} NMR spectra of silver(I) complexes **10-15** suggest the *N,Se,N*-chelating behaviour of the corresponding ligands towards the silver centre in solution. For thiazole-derivatives **11** and **12** this binding mode was confirmed by X-ray diffraction studies, while in hydrolysis product **15h**, the ligand presents a *N,Se*-bridging behaviour generating dimeric species in solid state.

The IR spectra brought evidence of the behaviour of the inorganic ligands - covalent in the case of complexes **10-15**, **17**, **20**, **24-25** and ionic in the case of complex **18** and **19**.

The ESI+ HRMS spectra of the silver(I) complexes show a base peak corresponding to $[LAg]^+$ fragment, while the copper complexes show the base peak corresponding to $[LCu]^+$ or $[LCu]^{2+}$ fragment.

Ligand **9** has a versatile coordination behaviour depending on the metal centre. It acts as *N,Se,N* chelating unit in the Cu(II) complexes **22-25**, resulting in the formation of monomeric species, and as bridging tetraconnective 2 x *N,Se* unit in complexes **18** and **20**, giving rise to polymeric species.

The silver(I) trifloromethanesulfonate complexes **10**-**12**, **15** and **18** and the silver(I) perchlorate complex **20** proved to be more active than the corresponding ligands and starting silver(I) salts against murine melanoma B16.F10 cells.

Subchapter III.3 focused on the use of the diorganodiselenide $(pzCH_2CH_2)_2Se_2$ (**26**) as a starting material for the synthesis of tin(IV) bis(organoselenolates) **27-30**, which were characterized by spectroscopic methods. Information on the coordination geometry of the tin(IV) atom in solution was obtained by calculating from NMR data the C–Sn–C angle for $Me_2Sn(SeCH_2CH_2pz)_2$ (**27**), $Bu_2Sn(SeCH_2CH_2pz)_2$ (**28**) and $Ph_2Sn(SeCH_2CH_2pz)_2$ (**29**). The results indicate a distorted tetrahedral coordination geometry around the tin atom in solution in all cases.

Compounds **26**, **27** and **30** proved to have a significant antiproliferative activity against murine colon carcinoma C26 cells, but the presence of tin did not improve the activity.

VI. SELECTED REFERENCES

47 M. Iwaoka and S. Tomoda, *J. Am. Chem. Soc.*, 1994, **116**, 2557–2561.
48 A. Panda, G. Mugesh, H. B. Singh and R. J. Butcher, *Organometallics*, 1999, **18**, 1986–1993.
52 A. Pop, D. Rosca, R. Mitea and A. Silvestru, *Inorg. Chim. Acta*, 2013, **405**, 235–242.
55 M. Iwaoka and S. Tomoda, *J. Am. Chem. Soc.*, 1996, **118**, 8077–8084.
58 J. Emsley, *Die Elemente*, Walter de Gruyter, Berlin, 1994.
66 A. A. Lysova, R. D. Marchenko, D. G. Samsonenko, A. S. Potapov and V. P. Fedin, *Russ. Chem. Bull. Int. Ed.*, 2020, **69**, 1122–1129.
68 M. David, R. Mitea and A. Silvestru, *J. Mol. Struct.*, 2021, **1246**, 131243.
74 V. Nascimento, E. E. Alberto, D. W. Tondo, D. Dambrowski, M. R. Detty, F. Nome and A. L. Braga, *J. Am. Chem. Soc.*, 2012, **134**, 138–141.
104 B. Danciu, R. Popa, A. Pop, V. Zaharia, C. Silvestru and A. Silvestru, *Stud. UBB Chem.*, 2016, **LXI**, 19–28.
105 R. A. Popa, E. Licarete, M. Banciu and A. Silvestru, *Appl. Organomet. Chem.*, 2018, **32**, e4252.
106 A. Gupta, R. Deka, R. J. Butcher and H. B. Singh, *Acta Crystallogr. Sect. C*, 2020, **C76**, 828–835.
107 A. L. Spek, *J. Appl. Crystallogr.*, 2003, **36**, 7–13.
108 A. L. Spek, *Acta Crystallogr. Sect. D*, 2009, **D65**, 148–155.
111 A. S. Hodage, P. P. Phadnis, A. Wadawale, K. I. Priyadarsini and V. K. Jain, *Org. Biomol. Chem.*, 2011, **9**, 2992–2998.
112 M. Iwaoka and F. Kumakura, *Phosphorus. Sulfur. Silicon Relat. Elem.*, 2008, **183**, 1009–1017.
118 K. B. Wiberg, *Tetrahedron*, 1968, **24**, 1083–1096.
120 R. N. Behera and A. Panda, *RSC Adv.*, 2012, **2**, 6948–6956.
121 B. K. Sarma and G. Mugesh, *ChemPhysChem*, 2009, **10**, 3013–3020.
122 L. Vogel, P. Wonner and S. M. Huber, *Angew. Chem., Int. Ed.*., 2019, **58**, 1880–1891.
123 W. Wang, B. Ji and Y. Zhang, *J. Phys. Chem. A*, 2009, **113**, 8132–8135.
124 S. S. Sadhu, S. Wang, R. K. Averineni, T. Seefeldt, Y. Yang and X. Guan, *Melanoma Res.*, 2016, **26**, 572–579.
125 Q. Y. Tong, Y. Qing, D. Shu, Y. He, Y. L. Zhao, Y. Li, Z. L. Wang, S. Y. Zhang, Z. H. Xing, C. Xu, Y. Q. Wei, W. Huang and X. H. Wu, *Cell. Physiol. Biochem.*, 2011, **27**, 233–242.
126 W. J. Geary, *Coord. Chem. Rev.*, 1971, **7**, 81–122.
127 I. Ali, W. A. Wani and K. Saleem, *Synth. React. Inorganic, Met. Nano-Metal Chem.*, 2013, **43**, 1162–1170.
128 A. Taurins, J. G. E. Fenyes and R. N. Jones, *Can. J. Chem.*, 1957, **35**, 423–427.
129 G. Zerbi and C. Alberti, *Spectrochim. Acta*, 1962, **18**, 407–423.
130 S. J. Angus-Dunne, L. E. P. Lee Chin, R. C. Burns and G. A. Lawrance, *Transit. Met. Chem.*, 2006, **31**, 268–275.
132 A. W. Addison, T. N. Rao, J. Reedijk, J. van Rijn and G. C. Verschoor, *J. Chem. Soc., Dalton Trans.*, 1984, 1349–1356.
133 T. K. Lal, R. Gupta, S. Mahapatra and R. Mukherjee, *Polyhedron*, 1999, **18**, 1743–1750.
134 L. Yang, D. R. Powell and R. P. Houser, *Dalton Trans.*, 2007, 955–964.
135 A. Okuniewski, D. Rosiak, J. Chojnacki and B. Becker, *Polyhedron*, 2015, **90**, 47–57.

136 M. Leboschka, M. Sieger, B. Sarkar, M. Niemeyer, T. Schurr, J. Fiedler, S. Záliš and W. Kaim, *Z. Anorg. Allg. Chem.*, 2009, **635**, 1001–1007.
140 S. S. Massoud, L. Le Quan, K. Gatterer, J. H. Albering, R. C. Fischer and F. A. Mautner, *Polyhedron*, 2012, **31**, 601–606.
141 S. S. Massoud, F. R. Louka, Y. K. Obaid, R. Vicente, J. Ribas, R. C. Fischer and F. A. Mautner, *Dalton Trans.*, 2013, **42**, 3968–3978.
142 K. Nakamoto, *Infrared and Raman Spectra of Inorganic and Coordination Compounds*, John Wiley & Sons, Inc., Chichester, Sixth Ed., 2008.
143 B. J. Hathaway and A. E. Underhill, *J. Chem. Soc.*, 1961, 3091–3096.
144 S. Azizzadeh, V. Nobakht, L. Carlucci and D. M. Proserpio, *Polyhedron*, 2017, **130**, 58–66.
149 X. Liang, S. Luan, Z. Yin, M. He, C. He, L. Yin, Y. Zou, Z. Yuan, L. Li, X. Song, C. Lv and W. Zhang, *Eur. J. Med. Chem.*, 2018, **157**, 62–80.
150 U. Kalinowska-Lis, A. Felczak, L. Chęcińska, I. Szabłowska-Gadomska, E. Patyna, M. Małecki, K. Lisowska and J. Ochocki, *Molecules*, 2016, **21**, 87.
151 A. F. Santos, I. P. Ferreira, C. B. Pinheiro, V. G. Santos, M. T. P. Lopes, L. R. Teixeira, W. R. Rocha, G. L. S. Rodrigues and H. Beraldo, *ACS Omega*, 2018, **3**, 7027–7035.
158 R. K. Sharma, G. Kedarnath, A. Wadawale, C. A. Betty, B. Vishwanadh and V. K. Jain, *Dalton Trans.*, 2012, **41**, 12129–12138.
159 A. Tyagi, A. Y. Shah, G. Kedarnath, A. Wadawale, V. Singh, D. Tyagi, C. A. Betty, C. Lal and V. K. Jain, *J. Mater. Sci.: Mater. Electron.*, 2018, **29**, 8937–8946.
160 A. Tyagi, G. Karmakar, A. Wadawale, A. Y. Shah, G. Kedarnath, A. P. Srivastava, V. Singh and V. K. Jain, *J. Organomet. Chem.*, 2018, **873**, 15–21.
161 A. Tyagi, G. Kedarnath, A. Wadawale, A. Y. Shah, V. K. Jain and B. Vishwanadh, *RSC Adv.*, 2016, **6**, 8367–8376.
162 M. D. Khan, M. Aamir, M. Sohail, M. Sher, N. Baig, J. Akhtar, M. A. Malik and N. Revaprasadu, *Dalton Trans.*, 2018, **47**, 5465–5473.
168 P. B. Hitchcock, M. F. Lappert, L. J.-M. Pierssens, A. V. Protchenko and P. G. H. Uiterweerd, *Dalton Trans.*, 2009, 4578–4585.
172 T. P. Lockhart and W. F. Manders, *Inorg. Chem.*, 1986, **25**, 892–895.
173 T. P. Lockhart, W. F. Manders and J. J. Zuckerman, *J. Am. Chem. Soc.*, 1985, **107**, 4546–4547.
174 J. Holeček and A. Lyčka, *Inorg. Chim. Acta*, 1986, **118**, L15–L16.
175 J. Holeček, K. Handlíř, M. Nádvorník and A. Lyčka, *Z. Chem.*, 1990, **30**, 265–266.

VIII. RESULTS DISSEMINATION

1. Roxana A. Popa, Emilia Licarete, Manuela Banciu, Anca Silvestru, Organoselenium compounds containing pyrazole or phenylthiazole groups: Synthesis, structure, tin(IV) complexes and antiproliferative activity, *Applied Organometallic Chemistry*, **2018**, *32*, *e*4252, DOI: 10.1002/aoc.4252 (Impact factor: 3.259, ISI Journal Citation Reports (Clarivate Analytics, 2019) © Ranking: 10/45 Chemistry, Inorganic & Nuclear, 17/71 Chemistry, Applied).

2. Roxana A. Popa, Vito Lippolis, Anca Silvestru, Cu(II) and Ag(I) complexes of the pyrazole-derived diorganoselenide $(pzCH_2CH_2)_2Se$. Synthesis, solid state structure and solution behavior, *Inorganica Chimica Acta*, **2021**, *520*, 120272, DOI: 10.1016/j.ica.2021.120272 (Impact factor: 3.118, ISI Journal Citation Reports (Clarivate Analytics, 2022) © Ranking: 19/46 Chemistry, Inorganic & Nuclear).

3. Roxana A. Popa, Adrian Nicoară, Massimiliano Arca, Vito Lippolis, Anna Pintus, Anca Silvestru, Homo- and heteroleptic diorganoselenides containing pyrazole functionalities. Synthesis, characterization and antioxidant activity, *Applied Organometallic Chemistry*, **2022**, *36*, *e*6894, DOI: 10.1002/aoc.6894 (Impact factor: 4.072, ISI Journal Citation Reports (Clarivate Analytics, 2022) © Ranking: 10/46 Chemistry, Inorganic & Nuclear, 23/72 Chemistry, Applied).

4. Roxana A. Popa, Maria David, Emilia Licarete, Manuela Banciu, Anca Silvestru, On the coordination behaviour of diorganoselenium ligands based on amino and azole functionalities: silver(I) complexes with relevance for biological applications, *New Journal of Chemistry*, **2022**, DOI: 10.1039/D2NJ04812D, *in press* (Impact factor: 3.925, ISI Journal Citation Reports (Clarivate Analytics, 2022) © Ranking: 80/179 Chemistry, Multidisciplinary).